Cell Systems

Article

Protein turnover regulation is critical for influenza A virus infection

Graphical abstract

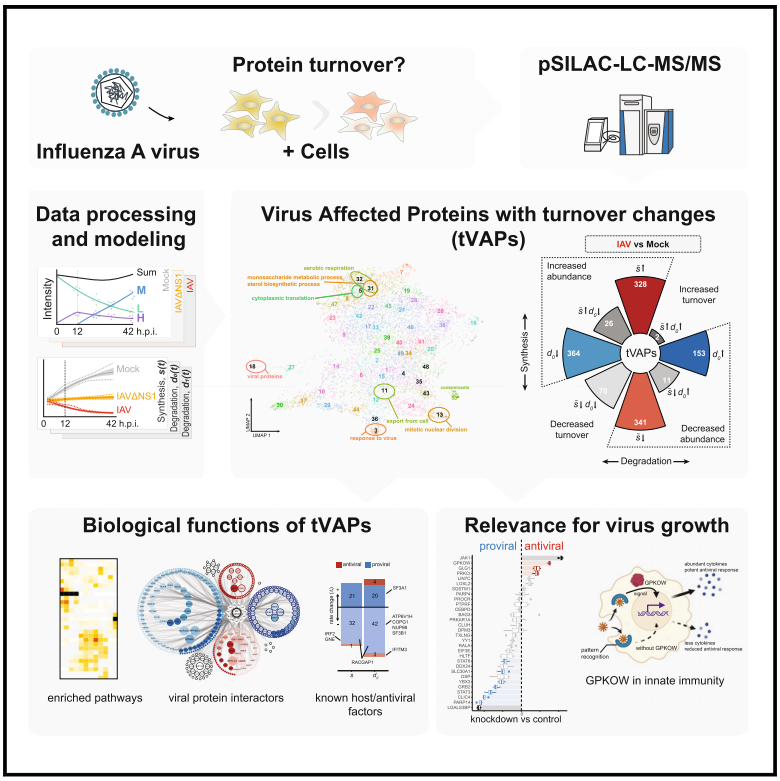

Authors

Yiqi Huang, Christian Urban, Philipp Hubel, Alexey Stukalov, Andreas Pichlmair

Correspondence

andreas.pichlmair@tum.de

In brief

Huang et al. analyzed protein synthesis and degradation in influenza A virus-infected cells using mass spectrometry and advanced Bayesian modeling. They found that protein turnover is an essential regulatory mechanism in virus-infected cells, which contributes to both virus replication and antiviral defense.

Highlights

- Influenza A virus infection extensively affects protein synthesis and degradation
- Proteins changing degradation are enriched with IAV interactors
- Loss-of-function analyses uncover previously unreported host and restriction factors
- The RNA splicing factor GPKOW is essential for inducing antiviral immunity

Huang et al., 2024, Cell Systems *15*, 911–929
October 16, 2024
https://doi.org/10.1016/j.cels.2024.09.004

CellPress

Cell Systems

CellPress
OPEN ACCESS

Article

Protein turnover regulation is critical for influenza A virus infection

Yiqi Huang,[1,6] Christian Urban,[1,6] Philipp Hubel,[2,6] Alexey Stukalov,[1,5] and Andreas Pichlmair[1,3,4,5,7,*]
[1]Institute of Virology, Technical University of Munich, School of Medicine, Munich, Germany
[2]Core Facility Hohenheim, Universität Hohenheim, Stuttgart, Germany
[3]Institute of Virology, Helmholtz Munich, Munich, Germany
[4]German Centre for Infection Research (DZIF), Partner Site, Munich, Germany
[5]Senior author
[6]These authors contributed equally
[7]Lead contact
*Correspondence: andreas.pichlmair@tum.de
https://doi.org/10.1016/j.cels.2024.09.004

SUMMARY

The abundance of a protein is defined by its continuous synthesis and degradation, a process known as protein turnover. Here, we systematically profiled the turnover of proteins in influenza A virus (IAV)-infected cells using a pulse-chase stable isotope labeling by amino acids in cell culture (SILAC)-based approach combined with downstream statistical modeling. We identified 1,798 virus-affected proteins with turnover changes (tVAPs) out of 7,739 detected proteins (data available at pulsechase.innatelab.org). In particular, the affected proteins were involved in RNA transcription, splicing and nuclear transport, protein translation and stability, and energy metabolism. Many tVAPs appeared to be known IAV-interacting proteins that regulate virus propagation, such as KPNA6, PPP6C, and POLR2A. Notably, our analysis identified additional IAV host and restriction factors, such as the splicing factor GPKOW, that exhibit significant turnover rate changes while their total abundance is minimally affected. Overall, we show that protein turnover is a critical factor both for virus replication and antiviral defense.

INTRODUCTION

Protein turnover, the interplay of protein synthesis and degradation, is fundamental to cellular homeostasis. Correlative studies comparing mRNA and protein abundance in cells estimate that mRNA levels can only partially explain protein abundance,[1–3] signifying the importance of measuring protein translation and degradation to understand its regulation. The correlation between mRNA and protein abundance is expected to vary considerably in cells perturbed by stimuli or infected with intracellular pathogens, such as viruses. Several pioneer studies revealed that treatments (e.g., lipopolysaccharide stimulation, oxidative, or osmotic stress) induce upregulation of proteins that can largely be explained by an increase in mRNA transcription, while the downregulation of proteins poorly correlated with mRNA level changes,[4–6] suggesting translational and post-translational mechanisms. Notably, proteins affected by stimuli via transcriptional regulation carried out distinct functions compared with proteins controlled on a translational or post-translational level.[6–9] Similarly, virus infection strongly influences protein turnover as the combined result of cellular responses to the virus infection and targeted interference of the virus with the cellular machinery. The regulation of protein turnover can occur at the protein synthesis stage through transcriptional, post-transcriptional, and translational changes or affect the protein half-life via, e.g., post-translational modifications (PTMs) and protein-protein interactions (PPIs).

Both the cellular response and virus interference dramatically affect the host protein synthesis during virus infection.[10–12] On the one hand, infected cells initiate the transcription and translation of antiviral proteins, which limit virus growth and trigger adaptive immune response.[13,14] Detection of viruses via pattern recognition receptors activates transcription factors like interferon regulatory factor (IRF) 3/7 and nuclear factor κB (NF-κB), which leads to the transcription and translation of mRNAs that encode cytokines, including interferons (IFNs).[15] IFNs activate signal transducer and activator of transcription (STAT) proteins and thereby induce the expression of IFN-stimulated genes (ISGs) with antiviral functions.[16,17] In addition to transcriptional control, translational regulation is particularly important for rapid and specific cellular responses to changing environments. Certain transcripts, such as the mRNA of the transcription factor IRF7, are translationally controlled during immunological responses.[18] Similarly, cytokines like IFN-γ[19] and interleukin-2 (IL-2)[20,21] bear RNA secondary structures contributing to their translational regulation. Moreover, proteins such as the translational regulator EIF2AK2 (PKR) generally inhibit cellular protein production but, in the context of pathogen infection, allow or

even promote—innate immune response.[22–26] On the other hand, viruses have developed numerous strategies to manipulate host protein synthesis to favor the expression of viral proteins and limit innate and adaptive immune responses. Many viruses inhibit global cellular protein synthesis through various mechanisms, which is commonly termed "host shutoff." For instance, D9/D10 proteins of the vaccinia virus induce the decay of host transcripts, effectively turning off their translation[27,28]; the NSP1 of severe acute respiratory syndrome coronavirus 2 (SARS-CoV-2) binds to the mRNA channel on the ribosome to specifically inhibit the translation of host mRNAs[29]; and the 2Apro and Lpro proteins of many picornaviruses directly cleave eIF4G to prevent translation initiation.[30,31] The importance of the host shutoff is exemplified by the non-structural protein 1 (NS1) and the endoribonuclease PA-X of influenza A virus (IAV). NS1 suppresses general eukaryotic transcription via the interaction with CPSF4,[32] a protein essential for proper mRNA polyadenylation. NS1 additionally inhibits the activation of retinoic acid-inducible gene I (RIG-I) and thus prevents the expression of antiviral cytokines.[33] By contrast, PA-X directly degrades host mRNA.[34] The NS1 and PA-X complement each other to effectively suppress the host response and promote IAV replication.[35] IAV strains lacking NS1 or bearing critical NS1 mutations are impaired in replication *in vitro* and attenuated *in vivo*,[36–38] and loss of PA-X expression has strain-dependent effect on the virulence of IAV.[39] Therefore, the protein synthesis machinery is one of the main battlegrounds for viruses and hosts, and the outcome of this struggle contributes to viral pathogenicity.

Besides regulation of protein synthesis, numerous examples show that virus infection substantially affects protein half-life. Intracellular processes, including protein degradation via the ubiquitin-proteasome system (UPS) and autophagy, membrane rearrangements, and induction of cell death through cell-intrinsic and extrinsic pathways, affect protein stability during virus infection.[40–42] The human genome contains around 600 putative E3 ligases,[43] which regulate diverse cellular processes by selectively targeting proteins for proteasomal or autophagolysosomal degradation, thus allowing highly dynamic regulation of protein abundance. For example, the signaling protein IkappaB needs to be degraded to activate NF-κB transcription factors as a part of the antiviral response.[44] By contrast, the transcription factor NRF2 is constantly ubiquitinated by the E3 ligase KEAP1 for degradation but stabilized upon oxidative stress or virus infection to initiate anti-inflammatory and antiviral responses.[45–47] ISG15 is induced by IFN and, as a PTM, can interfere with ubiquitination and thus alter the stability of host proteins to promote antiviral immunity.[48,49] For instance, IRF3 is ISGylated during Sendai virus infection to prevent its degradation via the UPS and sustain its activation.[50] As a countermeasure, many viruses express proteins that regulate proteasomal degradation to degrade critical innate immune factors, including IRF3,[51,52] which allows viruses to escape the innate immune response and spread efficiently.[53,54] Other examples of viral proteins that disrupt innate immune regulatory functions are the herpes simplex virus 1 (HSV-1) ICP0, a viral ubiquitin ligase that targets small ubiquitin-like modifier (SUMO)-conjugated proteins involved in intrinsic antiviral immunity,[55] and the V proteins of paramyxoviruses, which induce degradation of STAT proteins by assembling them into the V-dependent degradation complexes with host DDB1 and CUL4A.[56] Moreover, Tat protein of human immunodeficiency viruses (HIV) can employ HDM2 to target IRF1 for degradation.[57] Apart from signal transducers, viruses can also target restriction factors, exemplified by the degradation of APOBEC3G and BST-2 by the Vpr and Vpu proteins of HIV, respectively.[58,59] Therefore, protein degradation is yet another process fiercely contested by viruses and the host.

Collectively, the protein turnover changes in virus-infected cells are highly dynamic and often involve changes beyond the differential expression of cellular mRNA. However, the identification of such changes, especially in protein stability, was often incidental or driven by specific hypotheses. Conventional omics methods measure gene expression or protein abundance but do not provide information on the transcript or protein stability. Meanwhile, specialized mass spectrometry (MS) and computational analyses allow the unbiased assessment of protein turnover rates on a systems scale by utilizing pulsed stable isotope labeling by amino acids in cell culture (pSILAC).[60] In classical SILAC, cells are labeled with light (SILAC-L; Lys0 Arg0), heavy (SILAC-H; Lys8 Arg10), and medium-heavy (SILAC-M; Lys4 Arg6) amino acids and grown in different conditions. Mixtures of these labels can be analyzed by MS, which allows relative quantification of the same protein in the corresponding SILAC-labeled conditions. In pSILAC, cells are initially grown in the SILAC-L medium, which is switched to the SILAC-H medium after a given time point ("pulsed"). The incorporation of the SILAC-H label and simultaneous reduction of proteins with the SILAC-L label can be used to deduce translation and degradation rates, respectively. With pSILAC, it is possible to elucidate whether the upregulation of a protein is caused by its increased translation or by reduced degradation, as well as to detect changes in protein turnover rates that do not result in overall protein abundance changes. pSILAC has been successfully applied to study fundamental biological processes, such as cell differentiation[61] and complex assembly.[62,63] However, very few system-level studies used pSILAC to either characterize protein synthesis[64,65] or protein synthesis and degradation[66] during virus infection. One of the challenges is the analysis of the pSILAC data, in particular, decoupling system-level protein turnover changes due to host shutoff and cell growth inhibition from targeted changes of a particular protein.

Here, we employed a pSILAC approach with two SILAC medium switches ("pulse" and "chase") and advanced mathematical modeling to systematically profile the protein turnover change during the infection of IAV. We studied both the wild-type IAV strain SC35M and its mutant with deleted NS1 protein (IAVΔNS1), which is incapable of suppressing the host ISG response. Our analysis revealed that proteins from a wide range of biological processes are regulated by changes in synthesis, degradation, or the combination of both events during IAV infection, and we thus defined a group of virus-affected proteins that change their turnover (tVAPs). Notably, while their turnover is altered by the infection, many of the tVAPs demonstrate minimal changes in overall abundance. The integration of tVAPs with published IAV interactome and genome-wide functional screens identified that IAV infection alters the turnover of many important anti- and proviral proteins. The biological relevance of protein turnover changes was further validated using RNAi-mediated knockdown for selected proteins, identifying several host and

CellPress
OPEN ACCESS

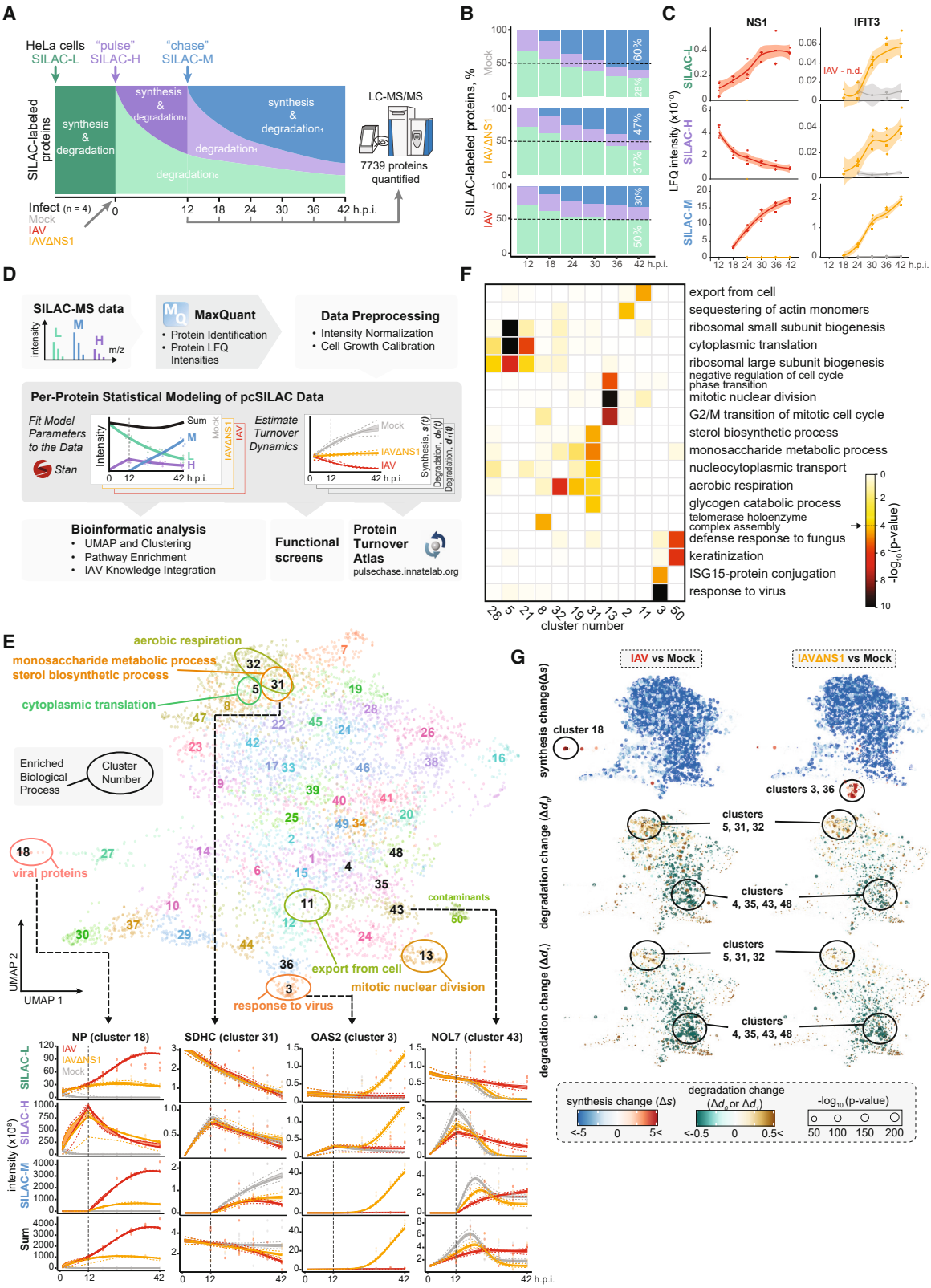

Figure 1. Profiling protein turnover changes in IAV-infected HeLa cells with pcSILAC proteomics

(A) pcSILAC experimental procedure. HeLa cells were grown in SILAC-L medium, infected with IAV or IAVΔNS1, and pulsed with SILAC-H medium until 12 h post-infection (h.p.i.), then chased with SILAC-M medium until 42 h.p.i. The samples were harvested every 6 h between 12 and 42 h.p.i. for mass spectrometry analysis.

(legend continued on next page)

restriction factors for IAV. Finally, we analyzed the mechanism of action of one restriction factor, G-patch domain, and KOW motifs-containing protein (GPKOW). We found that GPKOW influences the induction of type I IFN and, thus, the replication of IAV and other IFN-sensitive viruses. Altogether, these results highlight that shifts in the balance between synthesis and degradation of proteins constitute a crucial aspect of virus-host interaction during infection.

RESULTS

Protein synthesis and degradation in IAV-infected cells

To study protein turnover in virus infection, we used a pulse-chase SILAC (pcSILAC) metabolic labeling approach in HeLa cells infected with IAV. HeLa cells were the model system for multiple protein turnover studies[62,67,68] as they tolerate the switches of the growth medium well. We cultured HeLa cells in the SILAC-L medium and exchanged (pulsed) it with the SILAC-H medium immediately after the infection with IAV or IAVΔNS1. As a control, cells were left uninfected. The SILAC-L signal thus reflected the degradation of proteins that existed before the infection, while the SILAC-H signal represented proteins newly synthesized after infection. 12 h post-infection (h.p.i.), we substituted ("chased") the SILAC-H medium with the SILAC-M medium. After this point, the synthesis of SILAC-H-labeled proteins stopped, and degradation became the major factor that influences their abundance, while the newly synthesized proteins incorporated the SILAC-M label (Figure 1A). We harvested cells at 12, 18, 24, 30, 36, and 42 h.p.i. and analyzed the protein content using liquid chromatography coupled with tandem mass spectrometry (LC-MS/MS). Overall, we identified 7,739 proteins across all tested conditions (Table S1), of which more than 70% were quantified across all conditions based on label-free quantification (LFQ) values (Figures S1A and S1B). The total intensities of proteins with each SILAC label showed the expected distribution over time. More specifically, at 12 h.p.i., we could detect SILAC-H- and SILAC-L-labeled proteins, and the abundance of both labels decreased over time, while the intensity of SILAC-M-labeled proteins increased (Figure 1B). We detected a prominent reduction of SILAC-M incorporation in wild-type IAV-infected samples (30% vs. 60% in control experiment), which is likely due to host cell shutoff by the virus[69] (Figure 1B). The abundance of all detected viral proteins over time showed the accumulated SILAC-H-labeled proteins at 12 h.p.i. and the expected increase of SILAC-M-labeled proteins during the infection (Figure S1C), confirming progressive infection and specific incorporation of SILAC labels at the different experimental stages. Of note, NS1 was detected with all three SILAC labels at high intensities in the IAV infection but not IAVΔNS1 (Figure 1C). The strain-specific infection was further confirmed by the dynamics of classic antiviral proteins such as interferon-induced protein with tetratricopeptide repeats (IFIT) 3 and ISG15 (Figures 1C and S1D), which were abundantly expressed as SILAC-M-labeled proteins in the IAVΔNS1-infected but not IAV-infected cells. In addition, we observed a clear signal of viral proteins incorporating SILAC-L amino acids (Figure S1C), suggesting that these amino acids were likely recycled from the degraded SILAC-L-labeled host proteins.[70–73] The intensities of SILAC-L-labeled viral proteins at 42 h.p.i. increased up to 33-fold in comparison with the intensity at 12 h.p.i. during the wild-type IAV infection, which made up 1%–8% of the newly synthesized viral proteins at 42 h.p.i (Figure S1E). Amino acid recycling was also prominent for certain highly expressed ISGs (Figures 1C and S1D) in IAVΔNS1-infected cells.

To analyze this highly complex dataset, we established a statistical modeling approach, which allowed us to estimate the synthesis ($s(t)$) and degradation rates ($d(t)$) of individual proteins over time and in each of the tested conditions (Figure 1D). This model improved over the existing pSILAC data models[6] in several key areas: accounting for cell growth when modeling SILAC signal, nonlinear synthesis and degradation rates dynamics, and amino acid recycling (see STAR Methods for details). Moreover, by conducting both pulse and chase SILAC labeling steps, we were able to discern the degradation rates of proteins produced before [$d_0(t)$] and after the infection [$d_1(t)$]. This approach allowed us to compare protein turnover dynamics of all 7,739 proteins in uninfected and infected conditions (Table S2). For downstream system-level analysis, we used the total synthesis and degradation rates of individual proteins at each condition (s^i, d_0^i, d_1^i, where i = Mock, IAV, IAVΔNS1 denotes the infection type) for further comparisons between infection conditions (Table S2, see STAR Methods).

To identify general patterns in the dataset, we applied the UMAP[74] method to the protein intensity profiles and grouped proteins into 50 clusters based on the similarity of their pcSILAC dynamics in all infections (Figure 1E; Table S1). This analysis revealed a high diversity of turnover regulation and identified subsets of proteins with common turnover dynamics and biological functions (Figures 1E–1G). We found that cluster 18 contained proteins highly expressed after virus infection, particularly

(B) Percentage of summed LFQ intensities from proteins with each SILAC label at every experimental time point.
(C) LFQ intensities of NS1 and IFIT3 proteins in individual samples. The line indicates the mean LFQ intensity of the condition, and the shaded regions represent 95% confidence intervals. n.d., not detected.
(D) The pcSILAC data analysis pipeline.
(E) Above: UMAP of the diversity of protein turnover regulation based on the intensities of all three SILAC labels in IAV, IAVΔNS1, and control experiments (Table S1, PRIDE: PXD047063). Each dot represents one protein group, and the color and numeric label represent different clusters of protein turnover dynamics. Below: LFQ measurements and pcSILAC model estimated intensities of proteins from selected clusters with different SILAC labels in IAV, IAVΔNS1, and mock-infected cells. Dots indicate measured LFQ values from the MaxQuant output. The line indicates the modeled intensity median, and the shaded region and the dotted line represent 50% and 95% credible intervals, respectively.
(F) Non-redundant GO biological processes enriched in UMAP clusters. Each displayed term is significantly enriched at least in one cluster (unadjusted Fisher's exact test [FET] p value $\leq 10^{-4}$, indicated on the legend). Colors represent the p value in log scale (arbitrary units).
(G) Synthesis and degradation change (Δs, Δd_0, and Δd_1) of proteins in the UMAP between infected and mock conditions. Colors represent the direction and magnitude of change in linear scale (arbitrary units), and the dot size represents the $-\log_{10}(p$ value). Clusters with prominent synthesis or degradation changes are highlighted. n = 4 independent infections for all data in this figure.

CellPress
OPEN ACCESS

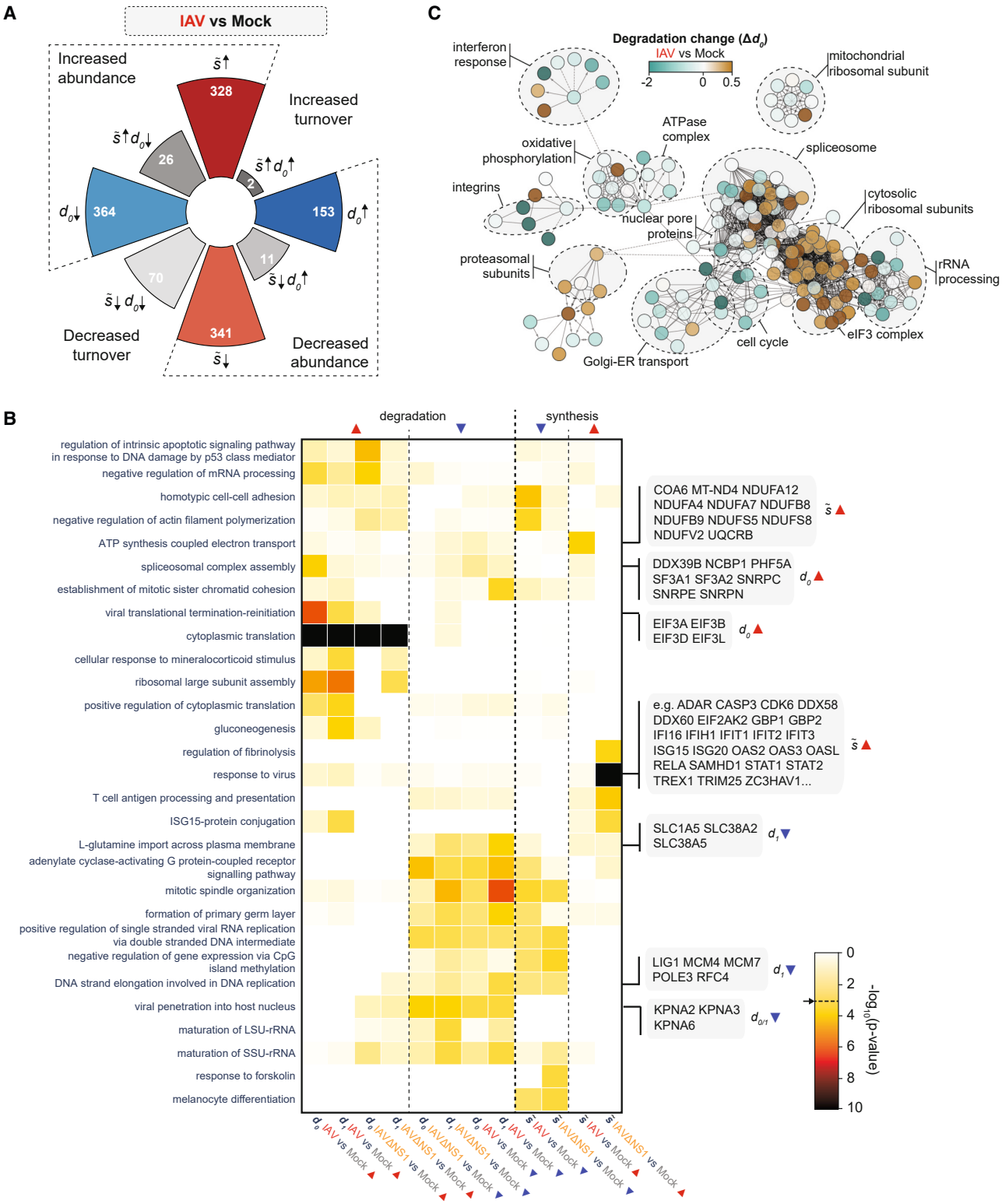

Figure 2. Pathway analysis of tVAPs in IAV infection

tVAPs are defined as proteins with significant synthesis or/and degradation changes in IAV or IAVΔNS1 infections (unadjusted p value $\leq$ 0.001 based on Bayesian modeling, $|\Delta\tilde{s}| \geq 1$, $|\Delta d_0| \geq 0.25$, or $|\Delta d_1| \geq 0.25$).

(A) Number of tVAPs that significantly changed synthesis, degradation, or both at the same time in IAV infection.

(legend continued on next page)

wild-type IAV (Figures 1E and 1G; Tables S1 and S2). This cluster contained all viral proteins and also cellular ones, for example, CLK3, which is involved in splicing,[75] and RABGAP1L, a restriction factor that potentiates ISG responses against RNA viruses and disrupts endocytosis[76] (Figure S1F). Clusters 3 and 36 contained proteins intensively synthesized in response to IAVΔNS1 infection but not the wild-type IAV. Cluster 3 was particularly enriched with proteins involved in the innate immune response (type I IFN signaling pathway, ISG15-protein conjugation, and protein mono-ADP ribosylation), such as IFITs, oligoadenylate synthetases (OASs), STATs, and ISG15/-20 (Figures 1E–1G and S1D). It additionally contained other proteins, such as COG6 and NT5E, that followed a similar expression pattern but were not classical ISGs (Figure S1G).

We could also identify clusters with infection-dependent changes in degradation (Figures 1E and 1G; Tables S1 and S2). However, unlike protein synthesis, degradation changes were common for IAV and IAVΔNS1 infections. The degradation rates of proteins existing before infection (d_0) and synthesized after infection (d_1) mostly changed in the same direction, with some differences in the magnitude (Figure S1H; Table S2). Proteins increasingly degraded during infection were primarily enriched in clusters 5, 31, and 32 (Figures 1E and 1G). These proteins were mostly associated with basic cellular functions such as cytoplasmic translation, metabolism, and intracellular transport (Figures 1E and 1F). Cluster 5 contained 42 of the 82 detected ribosomal proteins, and most of the remaining subunits were distributed among clusters 21, 22, 28, and 32 (Figure S1I). This coordinated degradation behavior may be explained by IAV-induced autophagosome targeting of the ribosome.[77] Contrary to the general trend, two ribosomal proteins (RPL7L1 and RPS27) localized to cluster 35 and were stabilized (i.e., their degradation was slowed down) (Figures S1I and S1J), suggesting a special role during IAV infection. Clusters 31 and 32 contained proteins relevant to metabolism, such as monosaccharide metabolic process, aerobic respiration, and sterol biosynthesis, all of which are modified and proven crucial during IAV infection.[78–81] Meanwhile, clusters 4, 35, 43, and 48 contained proteins stabilized upon infection (Figures 1E and 1G). In summary, besides recapitulating the expected regulation of protein synthesis elicited by IAV infection, our analysis of the pcSILAC data revealed other processes regulated by protein stabilization and degradation. Many proteins with similar turnover changes had similar biological functions, indicating the existence of coordinated processes.

IAV induces the alteration of protein turnover on the pathway level

The pcSILAC data revealed complex dynamics of protein turnover after IAV infection. Overall, the effect of the wild-type IAV virus was more prominent than that of the NS1-deleted strain, as reflected by the number of statistically significant (p value $\leq$ 0.001) infection-mediated changes in synthesis or degradation (Figure S2A). The total synthesis of proteins in the IAV-infected condition was much lower than in mock- or IAVΔNS1-infected cells. Most of these changes were likely due to the IAV-induced host shutoff (Figures 1B and 1G), differences in virus propagation (Figure S1C), and the role of NS1 in these processes.[32,82] To identify proteins specifically regulated within infected cells beyond the general trend, we corrected the synthesis rates ($\tilde{s}$) with respect to their median values in each condition (Figure S2A, STAR Methods). We further applied cutoffs to the magnitude of the corrected rate changes ($|\Delta\tilde{s}| \geq 1$, $|\Delta d_0| \geq 0.25$, and $|\Delta d_1| \geq 0.25$) to identify changes of higher biological relevance. Altogether, IAV and IAVΔNS1 infections significantly affected the turnover of 1,798 proteins, which we termed tVAPs (virus-affected proteins with turnover changes) (Figures 2A and S2B; Table S2). Over one-third of the changes overlapped between the two infections (Figure S2C). For IAV, we could identify 356 proteins with increased and 422 proteins with reduced synthesis rates, as well as 166 and 460 proteins with increased or reduced degradation (d_0) rates, respectively. For several tVAPs, increased synthesis was combined with stabilization, or vice versa, reduced synthesis was combined with faster degradation, resulting in synergistic effects on protein abundance. Prominent examples of tVAPs with such behavior are NDUFA7 and CSPG4 during both IAV and IAVΔNS1 infections (Figure S2D). A subset of tVAPs exhibited a simultaneous increase in synthesis and degradation, such as TRIM25 after IAVΔNS1 infection, or a decrease in synthesis and degradation, such as DDX56 after both IAV and IAVΔNS1 infections (Figure S2D). Such dynamics minimally affects the overall abundance of these tVAPs, but the change in turnover rates may indicate relevance for the infection. Notably, both TRIM25 and DDX56 have been described as being involved in antiviral immunity.[83,84] To validate the protein turnover changes derived from our model, we performed a pulse experiment using azidohomoalanine (AHA)/methionine as the metabolic labels. First, L-AHA is incorporated into newly generated proteins instead of methionine by culturing the cells in AHA-containing medium, and, after medium exchange to methionine-containing medium, the abundance of the AHA label in proteins reflects the stability of the protein. In this experimental setup, the cells were first labeled with L-AHA, and pulsed with medium containing methionine immediately after IAV infection. The AHA-labeled proteins were then precipitated at 12, 24, and 36 h.p.i., and the abundance of specific proteins was probed by western blotting. We could confirm that the protein CSPG4 was more degraded in IAV-infected cells as compared with controls. Similarly, we found reduced degradation for STAT1 and IFITM3 in infected vs. uninfected cells. In addition, this approach faithfully recapitulated recycling of amino acids for the production of viral proteins, which we also saw in the SILAC-pulse-chase data (Figure S2E).

To identify pathways affected by protein turnover, we applied gene set enrichment analysis to tVAPs grouped by their synthesis and degradation changes. In general, IAV and IAVΔNS1 infections affected similar pathways distinctively regulated by synthesis and degradation (Figure 2B; Table S2). For example,

(B) Non-redundant GO biological processes enriched in tVAPs with up- or down-regulated synthesis or degradation rates during IAV or IAVΔNS1 infections (unadjusted FET p value $\leq$ 0.001, indicated on the legend). Colors represent the p value in log scale (arbitrary units).
(C) Gene set expression analysis of tVAPs with significant d_0 changes in IAV infection via ReactomeGSA. Reactome pathways significantly enriched in each cluster were shown (false discovery rate [FDR] $\leq$ 0.001). Colors represent the direction and magnitude of d_0 change in linear scale (arbitrary units).

proteins of mitotic spindle organization were regulated by both reduced degradation and synthesis, whereas proteins that negatively regulate gene expression via methylation were mostly less synthesized. Many proteins involved in cytoplasmic translation were more degraded, but the proteins involved in the maturation of large and small subunit ribosomal ribonucleic acid (LSU and SSU rRNA) were stabilized, particularly those produced after the infection ($\Delta d_1 < 0$). We found that many biological processes previously described to be affected by IAV infection are regulated by protein stabilization or degradation. For instance, the importin subunits involved in viral penetration into the host nucleus (KPNA2/3/6) were stabilized (Figure 2B; Table S2), and KPNA2/3/6 are crucial for IAV replication in different host species.[85–87] Similarly, the solute carrier proteins involved in glutamine import (SLC1A5, SLC38A2, and SLC38A5) were stabilized, potentially explaining a previous report on the increased glutamine uptake by IAV-infected cells.[88] Although an RNA virus, IAV also relies on the components of host DNA replication machinery to replicate its genome,[89] which may be reflected by the stabilization of proteins involved in DNA strand elongation. In addition, some pathways were specifically regulated by IAV or IAVΔNS1 infection. As expected, many ISGs were synthesized after IAVΔNS1 but not after IAV infection, in line with the known immune-suppressive function of NS1.[90,91] Conversely, in IAV infection, but not when infecting with IAVΔNS1, many proteins participating in oxidative phosphorylation (ATP synthesis coupled electron transport) maintained high synthesis rates. This agrees with previously observed differential expression of these genes in IAV- and IAVΔNS1-infected cells[69,92] and suggests that NS1 is relevant for ensuring energy production during IAV infection. We could also observe virus-specific pathway perturbation through altered protein degradation. For example, IAV infection led to increased degradation of eIF3 complex subunits (EIF3A/B/D/L) associated with viral translational termination reinitiation, as well as a complex regulation of spliceosome complex subunits (eight more degraded and nine stabilized) (Figure 2B; Table S2).

We noticed that some tVAPs involved in the same biological process were regulated in opposite directions. To systematically identify regulatory processes with heterogeneous turnover changes, we used another gene set enrichment method (ReactomeGSA[93]) that enabled us to assess the magnitude and direction of degradation changes (Δd_0) of tVAPs that belonged to the same pathway (Figures 2C and S2F; Table S2). This analysis revealed the regulation of individual tVAPs that behaved differently from the general trend of their protein complex or process. For instance, while many proteins involved in oxidative phosphorylation were stabilized, the subunit NDUFS6 was more degraded. Unlike the cytosolic ribosome, the stability of the mitochondrial ribosomal subunits was mostly unaffected or even improved, which may partially explain the minimally affected translation of the electron transport chain proteins (Figure 2B). However, a single component of the large subunit, MRPL4, was increasingly degraded. Proteins involved in Golgi-ER transport were stabilized, except TMED2, which was degraded. TMED2 has been reported to have an antiviral function in a knockdown screen of IAV interactors.[94] It was further identified to facilitate STING activation,[95] which plays an important role in controlling IAV propagation.[96] These results demonstrate that IAV infection profoundly perturbs cellular pathways by modulating protein synthesis, degradation, or both. Moreover, the discordant regulation of individual complex members may indicate specific viral targeting of key proteins that are relevant for the activity of the respective protein complex or an adaptation of the cell to the infection.

Altered stability of cellular proteins interacting with IAV

To elucidate regulatory principles causing the differential turnover of tVAPs during IAV infection, we first intersected our data with reported PPIs of IAV proteins from five independent studies[94,97–100] (Table S3). Among the 1,414 tVAPs induced by IAV infection, 566 were reported interactors of IAV proteins (Figure 3A; Table S3). Within these 566 tVAPs, there was a striking overrepresentation of proteins with altered degradation (Figure 3B). In addition, proteins that changed degradation rates during IAV infection were significantly enriched for interactors of IAV proteins (Figure 3C). Conversely, tVAPs that have not been reported as IAV interactors showed a profound overrepresentation of proteins with changed synthesis rates (Figure 3B), and there was no significant enrichment of IAV-interacting proteins among proteins changing synthesis in IAV infection (Figure 3C). The above observation shows that interactions between viral and cellular proteins will likely affect their half-life in infected cells.

To investigate the functional relevance of the IAV-interacting tVAPs, we projected turnover changes during IAV infection onto a network of viral-host protein interactions (Figure S3A). As expected (Figures 3A–3C), this network is enriched for proteins with changes in degradation (343 proteins, blue nodes), while a smaller portion (216 proteins, red nodes) demonstrate altered synthesis (Figure S3A). The simultaneous binding and regulation of protein synthesis could have pronounced effects on the affected pathways. For example, IAV has been reported to arrest the cell cycle at G0/G1 to facilitate its replication.[101,102] Indeed, some IAV interactors with suppressed synthesis participate in the G2/M phase checkpoint (FANCI, INTS3, and KNTC1),[103–105] mitosis (ANAPC7, CKAP5, NCAPG, SMC4, TOP2A, TOP2B, and USP9X)[106–110] or G1 arrest (WDR6),[111] while GADD45GIP1, an inhibitor of the G1 to S progression,[112] was more synthesized (Figure S3B; Table S3). Seven of these differentially synthesized cell-cycle proteins have been identified more than once as interactors with the M2 protein. M2 also interacts with SPTLC1, a subunit of the serine palmitoyltransferase complex involved in *de novo* ceramide biosynthesis that suppresses IAV replication.[113] The downregulation of SPTLC1 synthesis and its interaction with M2 may thus synergistically reduce ceramide production to promote IAV replication. Another M2 interactor, TMX3, was minimally affected by the host shutoff. TMX3 catalyzes the formation of disulfide bonds[114] critical for the stability of the M2 channels,[115] which may explain its preserved synthesis during IAV infection.

Among the IAV interactors with altered degradation rates, many have critical functions in the replication cycle of the virus (Figures 3D–3F). For example, tVAPs involved in nucleocytoplasmic transport have been identified as IAV interactors by several studies.[94,97–100] Among them, the nuclear pore complex (NPC) proteins were commonly found to interact with M2, and the proteins of the NPC inner ring (NUP205, NUP188, and NUP155)

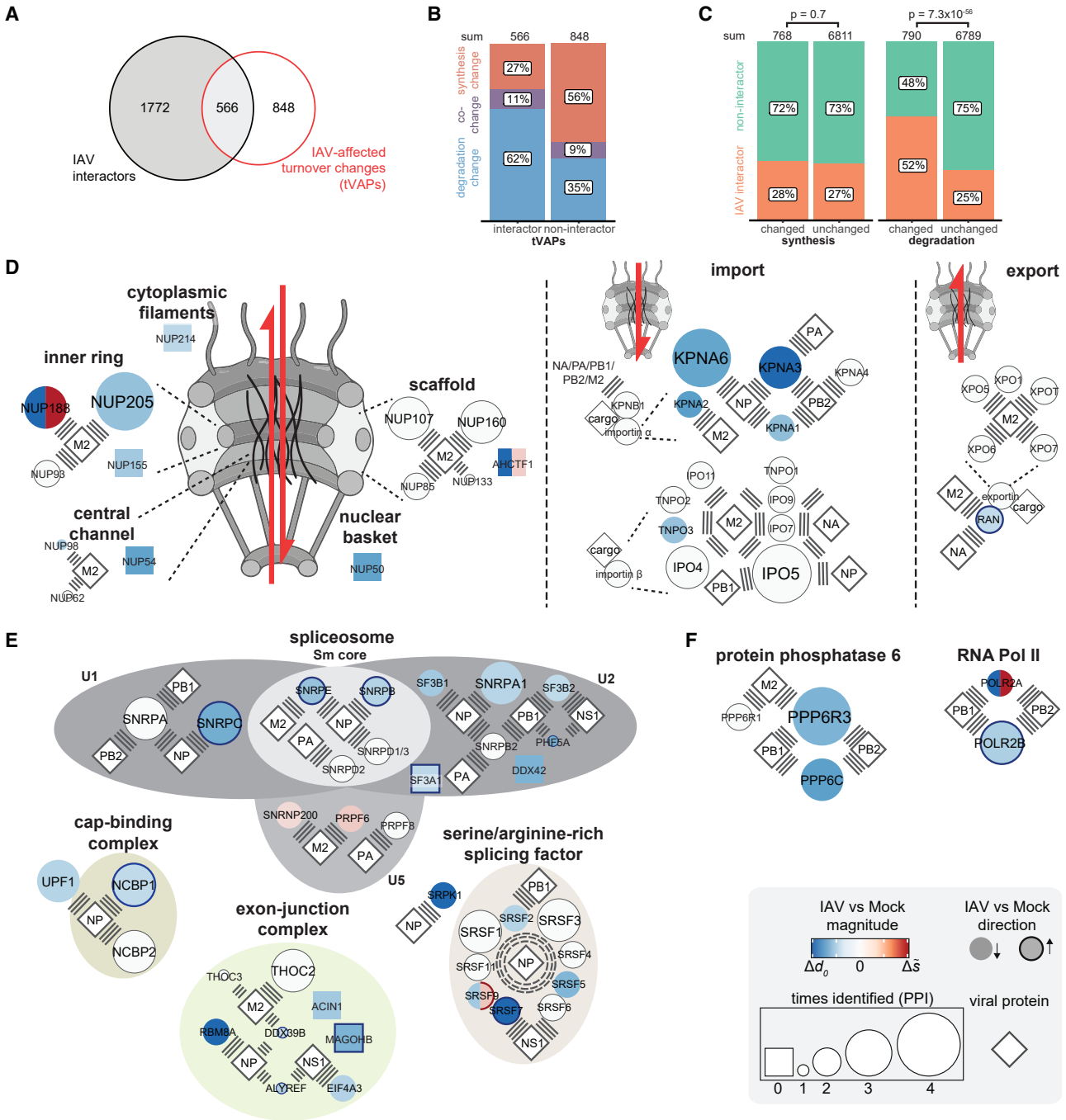

Figure 3. Integration of IAV-induced turnover changes and IAV host-virus interactome

(A) The overlap between tVAPs identified in IAV infection in our study and IAV interactors from five published studies.[94,97–100]

(B) Percentage of proteins with significant synthesis or degradation changes among tVAPs from IAV infection that are IAV interactors and not IAV interactors.

(C) Enrichment of IAV interactors among tVAPs with synthesis or degradation changes during IAV infection. FET *p* values are displayed.

(D–F) tVAPs and IAV interactors that participate in host pathways important for IAV replication. The color of the protein indicates the type ($\Delta\tilde{s}$ or Δd_0) and magnitude of change in linear scale (arbitrary units), and the border (with/without) indicates the direction of change during IAV infection in our study. The shape and size of the protein indicate the number of reported independent identifications of a host protein as an interactor of a viral protein. When multiple viral interactors of the host protein are shown, the most identified interaction pair determines the size of the circle. In general, only protein-protein interactions with more than one identification are displayed unless the host interactor is also a tVAP or the viral protein has other confident interactions within the depicted host pathway.

(D) tVAPs and IAV interactors involved in nucleocytoplasmic transport. The nuclear pore complex was created in BioRender. Pichlmair (2024), BioRender.com/o33o378.

(E) tVAPs and IAV interactors involved in splicing.

(F) tVAPs and IAV interactors involved in viral RNA replication.

were particularly stabilized (Figure 3D). Notably, NUP205 is also a host factor for IAV.[116,117] Moreover, among all the IAV-interacting importins and exportins, several importin-α proteins (KPNA1/2/3/6) were stabilized. The meta-analysis also highlighted other IAV-interacting tVAPs involved in viral RNA replication (Figure 3F), such as subunits (PPP6C, PPP6R3) of the protein phosphatase 6[118] and POLR2A and POLR2B[119] of the RNA polymerase II. Furthermore, our analysis revealed extensive interaction between viral proteins and tVAPs of host splicing machinery (Figure 3E). IAV relies on the host splicing machinery to produce NS2 and M2[120] and, in return, influences the splicing of host genes in favor of its own replication.[121,122] Within the spliceosome, subunits of U1 and U2 were identified as both tVAPs and IAV interactors. This may reflect the pivotal role of U1 and U2 in intron definition[123] and IAV's preference for U1 and U2 snRNAs as cap-snatching sources.[124] In particular, NP alone interacted with most of the serine/arginine-rich splicing factors (SRSFs) and their kinase (SRPK1), among which SRSF2/5/7/9 and SRPK1 are tVAPs, and SRSF5 was shown to mediate the splicing of the M gene.[125]

In summary, we found that host protein stability in IAV-infected cells was likely influenced by its ability to interact with viral proteins. Notably, among tVAPs that are differentially stabilized or degraded, many have known viral protein interactors and are involved in the replication cycle of IAV. Therefore, we expect additional yet uncharacterized host and restriction factors for IAV among the tVAPs identified during IAV infection.

Loss-of-function analysis identifies additional IAV host and restriction factors

In order to globally assess the functional importance of tVAPs, we further intersected our data with ten published genome-wide screens for IAV host and restriction factors[116,126–134] (Figure S4A; Table S3). Both the anti- and proviral proteins exhibited diverse turnover alterations in our pcSILAC data. tVAPs changing degradation rates, but not synthesis rates, were enriched in factors influencing IAV propagation (Fisher's exact test [FET] p value = 4.4×10^{-4} and 1, respectively). For example, the IFN-stimulated protein IFITM3, a well-described IAV restriction factor,[126] was stabilized upon infection, while its synthesis rates did not change significantly (Figure S2E). This phenotype may reflect the general inhibition of the ISG response by IAV[90,135,136] and aligns with the stabilization of IFITM3 in other virus infections due to reduced lysosomal degradation.[137] Members of the U2 small nuclear ribonucleoprotein particle (snRNP) complex like SF3A1, SF3B1, and SF3B2 were identified to be proviral, likely reflecting the important role of U2 during splicing of the viral RNA and as the cap donor during IAV mRNA synthesis.[124] Our analysis showed that SF3A1 was more degraded, while SF3B1 and SF3B2 were stabilized in IAV-infected cells. SF3B1 and SF3B2 were shown to interact with several IAV proteins in previous studies[94,97,99] (Figure 3E). Some proteins likely involved in IAV entry also changed synthesis or degradation, such as GNE, a regulator of N-acetylneuraminic acid synthesis,[138] and ATP6V1H, a subunit of the vacuolar ATPases.[139] The intersection between protein turnover change and previous functional studies further supported the notion that a change in protein turnover may indicate the protein's functional involvement during IAV infection.

To gain further insight into the role of tVAPs in IAV replication, we performed two small interfering RNA (siRNA)-mediated knockdown screens in HeLa cells for 28 tVAPs with diverse turnover dynamics after IAV and/or IAVΔNS1 infection (Figure 4A; Table S4). Additionally, we included two known pro- and anti-IAV factors, LGALS3BP[140] and JAK1,[135,141] and non-targeting (scrambled) siRNAs as controls. The control proviral factor LGALS3BP was also stabilized during IAV infection. We confirmed that the depletion of the individual proteins did not affect cell viability for most of the targets, apart from BAG3 and SQSTM1 (Figure S4B). We then used an IAV-Renilla reporter virus in the first screen, where the reporter signal reflects the propagation of the virus, to assess the effect of the candidates' knockdowns on virus growth. As expected,[140] compared with non-targeting controls, LGALS3BP depletion reduced, while the knockdown of JAK1 increased the Renilla signal, thus confirming the effective knockdown approach and expected behavior of controls in this system (Figures 4B and S4C). In total, we found that 10 of the 28 tested tVAPs significantly changed the Renilla signal (Figures 4B and S4C, adjusted p value ≤ 0.05, Welch's t test). We further employed an IAV mini-replicon system (based on the strain WSN) in the second screen, where the Firefly signal correlates with the replication of viral RNA. In this system, 14 proteins were found to be pro or antiviral (Figures 4B and S4C, $|\log_2 \text{FC}| \geq 0.5$ in at least two biological replicates). Since the replicon system only measures viral RNA replication, tVAP knockdown solely significant in the reporter virus screen but not the replicon screen suggests the role of this tVAP in virus entry or egress (e.g., PRKCI, PARP14, SLC30A1, GLG1, and YBX3). The knockdowns of GRB2 and STAT6 induced opposite phenotypes in the IAV-Renilla infection and the IAV-mini-replicon screens, underlining their potential differential involvement at various stages of viral life cycles. In addition, the knockdown of STAT3 and CLIC4 decreased the mini-replicon-driven luciferase signals, and the knockdown of GPKOW consistently increased the luciferase activity in both assays (Figures 4B and S4C). Among them, the turnover changes of STAT3 synergistically reduced its total abundance (Figure S4D), whereas, for CLIC4 and GPKOW, their total abundances barely changed during IAV infection (Figures 5A and S4E). In brief, the intersection with genome-wide siRNA screens and our loss-of-function experiments confirmed that alteration of turnover during IAV infection is an indication that a protein is likely an IAV host or restriction factor.

GPKOW—An antiviral immune modulator

In addition to the two knockdown screens, we could further confirm the antiviral phenotype of a splicing factor GPKOW[142,143] in lung-derived A549 cells (Figures S4F and S4G). While the IAV infection significantly slowed down the turnover of GPKOW, it had very little effect on GPKOW's total abundance (Figure 5A). Such a protein would not be revealed if only the absolute protein abundance is measured. To explore the underlying antiviral mechanism of GPKOW, we first compared the proteome of siRNA-mediated GPKOW knockdown to the control scrambled siRNA-treated HeLa cells during IAV-Renilla infection. Among 5,986 proteins quantified by LC-MS/MS, 316 showed differential expression (Figures S5A and S5B; Table S5). GPKOW was significantly downregulated in the GPKOW knockdown samples, confirming successful gene depletion. Moreover, we identified the downregulation of many proteins involved in antiviral

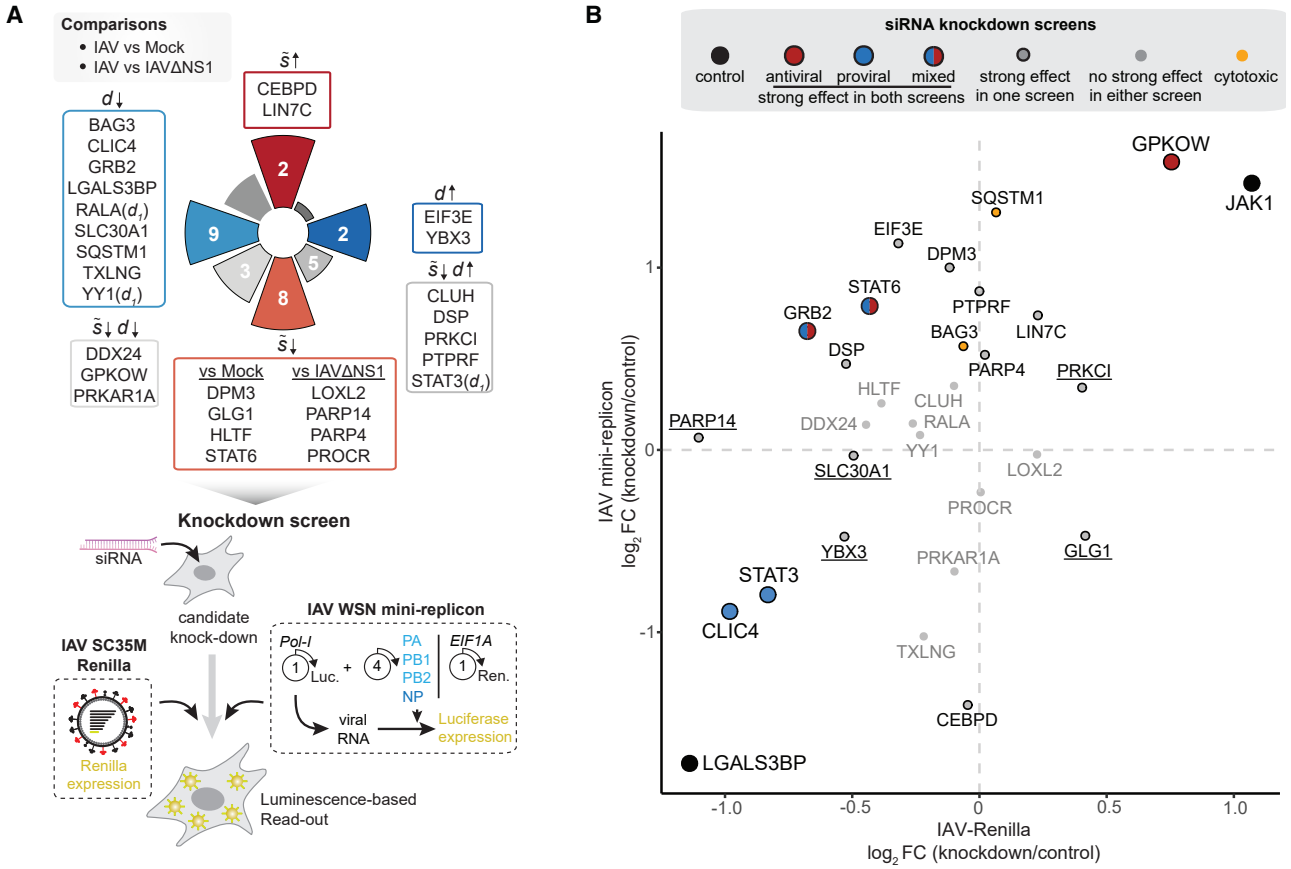

Figure 4. Identification of IAV host and restriction factors among tVAPs

(A) Candidate selection and the design of the loss-of-function screens. tVAPs were selected from the IAV vs. mock comparison unless otherwise stated (vs. IAVΔNS1). The degradation (d) changes generally apply to both d_0 and d_1 unless otherwise stated (d_1).

(B) $\log_2$ fold change (FC) of the luminescence signals between the cells with target gene knockdown and the control in the screens using IAV-Renilla or IAV mini-replicon. Strong effect (thick border) is defined as Benjamini-Hochberg (BH)-adjusted p value ≤ 0.05 in two-sided Welch's t test for the screen with IAV-Renilla ($n = 4$ independent wells) or $|\log_2 \text{FC}| \geq 0.5$ in at least two out of three independent experiments with IAV mini-replicon. Knockdowns with only strong effects in the IAV-Renilla infection were underscored. The knockdown is cytotoxic (yellow fill) when the knockdown cells have less than 80% of the viability of the scrambled controls and the BH-adjusted p value ≤ 0.05 ($n = 4$ independent wells).

immunity (Figure S5B, blue). Particularly notable was the reduced expression of several viral restriction factors (e.g., IFITs, EIF2AK2/PKR, and OASs) and innate immunity signaling molecules (STAT1 and IRF3). To confirm this phenotype and to clarify whether GPKOW is specifically required to mount an innate immune response, we further generated GPKOW knockdown cells using CRISPR-Cas9-mediated gene disruption in A549 cells. We then treated the GPKOW knockdown and control cells with either triphosphorylated dsRNA (PPP-RNA), a synthetic RIG-I agonist, or recombinant IFN-α, and subjected the samples for LC-MS/MS analysis, where 6,954 proteins were quantified (Figures 5B and S5C–S5E; Table S5). In control cells, both PPP-RNA and IFN-α induced strong expression of known ISGs and other proteins involved in antiviral immunity (Figure S5D). Notably, most protein expression changes identified in infected GPKOW knockdown cells were recapitulated upon PPP-RNA-, but not IFN-α-stimulated GPKOW knockdown cells (Figures 5B and S5E), indicating that GPKOW is relevant for the activation of the innate immune system. GPKOW knockdown further suppressed the production of IFN-α upon PPP-RNA stimulation (Figure 5C). Since the GPKOW depletion appeared to affect the activation of innate immune responses, we investigated its general relevance for other virus infections. We infected CRISPR-Cas9-mediated GPKOW knockdown cells with recombinant SFV expressing mCherry or VACV expressing GFP and monitored virus growth using live-cell imaging over 72 h (Figures 5D and S5F). The SFV-mCherry signal was significantly increased in GPKOW knockdown compared with control cells (Figure 5D, left). A similar effect of GPKOW depletion can be observed in VACV-GFP signal as compared with controls (Figure 5D, right). Altogether, our data characterized GPKOW as a co-factor to induce innate immune responses, but it is likely dispensable for signaling downstream of IFN-α. Moreover, GPKOW has a prominent antiviral function against different viruses, which could be explained by its role as an immune modulator (Figure 5E).

DISCUSSION

Here, we employed pcSILAC MS and advanced statistical modeling to track the synthesis and degradation of thousands

CellPress
OPEN ACCESS

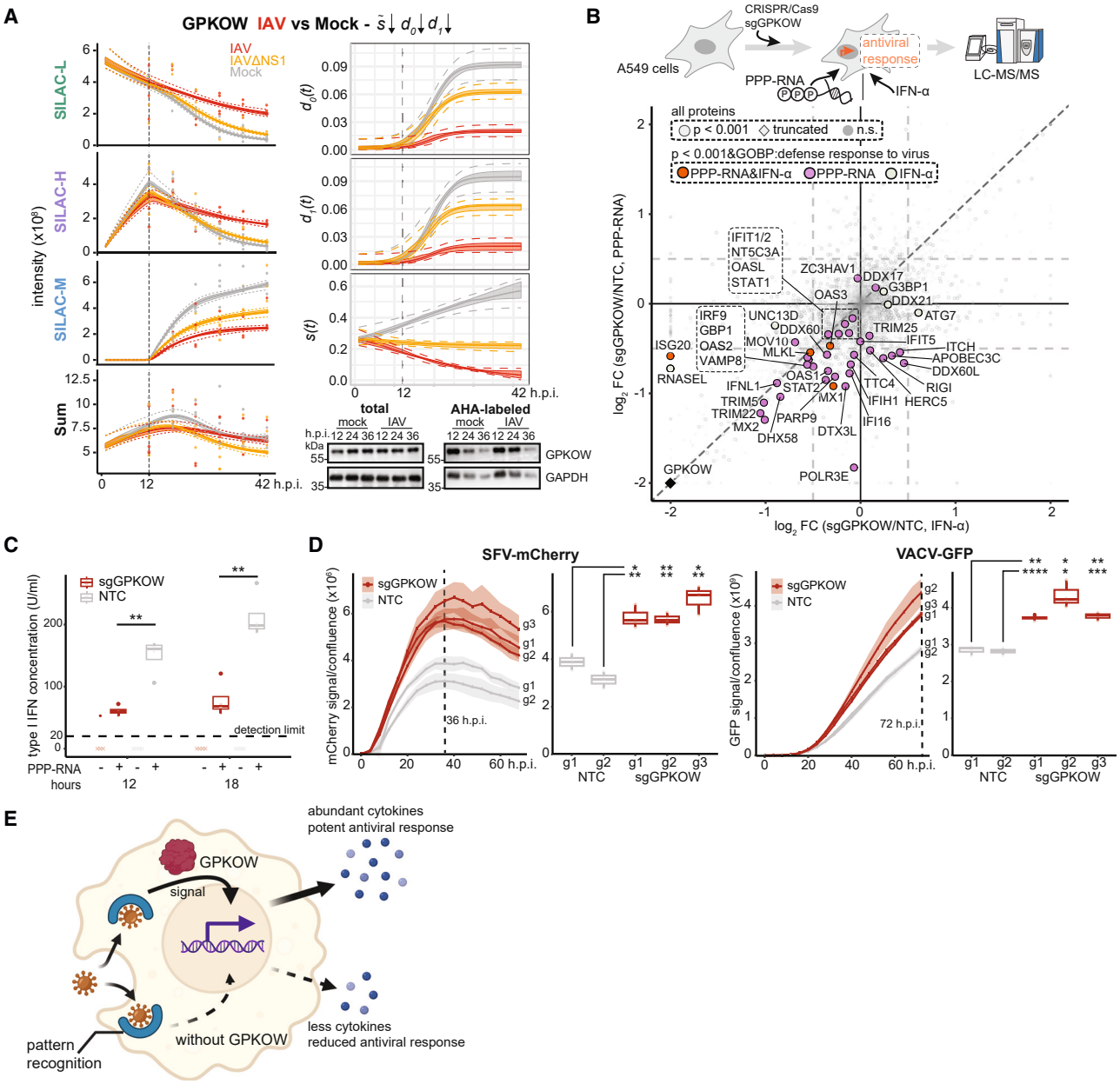

Figure 5. Involvement of GPKOW in innate immune responses

(A) Left: LFQ measurements and pcSILAC model estimated GPKOW intensities of different SILAC labels in IAV, IAVΔNS1, and mock-infected cells. Dots indicate measured LFQ values from the MaxQuant output. Right: model-estimated turnover rates of GPKOW. The line indicates the modeled intensity or rate median, and the shaded region and the dotted line represent 50% and 95% credible intervals, respectively ($n = 4$ independent infections). Bottom: degradation of AHA-labeled GPKOW in mock- or IAV-infected HeLa cells in AHA-methionine pulse experiments ($n = 3$ independent infections).

(B) The proteome changes between GPKOW knockdown A549 cells and control under PPP-RNA (y axis) or IFN-α (x axis) stimulation (Table S5, PRIDE: PXD047060). Protein abundance changes with unadjusted p value $\leq 10^{-3}$ in either comparison (based on Bayesian modeling) are marked with a border, and the proteins that belong to the GO "defense response to virus" process are highlighted ($n = 4$ independent wells). The $\log_2$ fold change (FC) cutoff is displayed as dashed horizontal or vertical lines, and the dashed diagonal line indicates y = x.

(C) Production of type I IFN in GPKOW knockdown A549 cells and non-targeting controls (NTC) after stimulation of PPP-RNA for the stated time ($n = 4$ independent wells, one representative experiment out of two is displayed).

(D) SFV and VACV replication in GPKOW knockdown A549 cells and NTCs analyzed by live-cell imaging. The line indicates the condition mean, and the shaded region represents mean ± SD. The boxplots show data at 36 h.p.i. for SFV and 72 h.p.i. for VACV, as marked by the dotted line in the line plots ($n = 3$ independent wells per experiment, and one representative experiment out of three is displayed). For (C) and (D), *p value ≤ 0.05; **p value ≤ 0.01; ***p value ≤ 0.001, ****p value ≤ 0.0001 with Welch's t test and BH p value adjustment.

(E) The proposed role of GPKOW that it participates in the activation of innate immune responses. (E) was created in BioRender. Pichlmair (2023), BioRender.com/b48k397.

of proteins during IAV infection. Our analysis of this yet largely unexplored aspect of virus-host interaction has revealed hundreds of tVAPs (Figures 2A and S2B; Table S2). These tVAPs were enriched in a wide range of biological pathways (Figures 2B and 2C), some of which are known to be modified by IAV replication. Many tVAPs with altered stability are known interactors of IAV proteins (Figure 3) or have pro- or anti-IAV roles in published studies and our loss-of-function analysis (Figures 4 and S4). Collectively, these findings highlight the biological importance of tVAPs in IAV infection.

Among the numerous alterations of protein turnover, IAV infection prominently changed degradation rates of a large number of proteins that are involved in splicing,[121,122] translation,[144,145] cell cycle,[101,102] and energy production.[146–148] The affected processes often involve the formation of large protein complexes. In our data, we observed both concordant and discordant turnover regulations of protein complex subunits, which may reflect the modulation of protein complex composition, structure, and function (Figures 2C and S2F; Tables S2 and S3). For example, 8 of the 13 subunits of the eIF3 complex involved in translation initiation were more degraded, and we observed coordinated degradation of cytosolic ribosomal subunits during IAV infection (Figures 1E, S1I, 2B, 2C, and S2F; Table S2). Further experiments are required to clarify whether the stability changes of the cytosolic translation machinery are a part of the cellular defense or, on the contrary, contribute to the preferential translation of the viral mRNAs. By contrast, the mitochondrial ribosomal subunits were mostly unaffected or even stabilized in our analysis (Figures 2C and S2F; Table S2). The opposite turnover regulation of mitochondrial ribosomes may help maintain the production of essential components of the respiratory chain[149] and ensure continuous activity of the oxidative phosphorylation pathway, which IAV requires for efficient propagation.[69] Apart from the changes in the translation machinery that may affect protein synthesis, we also identified tVAPs from the major protein degradation pathways.[150] The immunoproteasome subunits PSMB8, 9, and 10 were specifically more synthesized in IAVΔNS1-infected cells (Table S2), as expected from the active IFN signaling.[151] PSMA3, PSMB4, and PSMB5, members of the 20S proteasome core, were more degraded after IAV infection, while the rest of the conventional 20S core showed no significant changes (Figure S2E). This differential degradation of specific subunits may indicate the reshaping of the proteasome or result from their involvement in additional functions outside of the proteasome. PSMB4 was found to directly interact with the NS1 protein of IAV and to target it for proteasome-independent degradation.[152] It may be that PSMA3 or PSMB5 are similarly involved in the degradation of specific viral proteins. The changes in the abovementioned cellular processes will likely, in return, affect the turnover of other cellular and even viral proteins.

The regulation of tVAPs may be a cell-intrinsic function or be due to direct virus engagement. Indeed, we found that tVAPs with changed stability during infection were highly enriched for interactors of viral proteins (Figures 3B and 3C), and many IAV-interacting tVAPs are involved in cellular processes important for the viral life cycle (Figures 3D–3F). For example, our analysis revealed the increased stability of the catalytic core of protein phosphatase 6 (PPP6C) and one of its regulatory subunits (PPP6R3) during IAV infection (Figure 3F). These two proteins were previously reported to interact with PB1 and PB2 and are crucial for viral RNA replication.[118] PB1 and PB2 also interact with the two largest subunits of Pol II that together form the polymerase active center; POLR2A was more stabilized, while POLR2B was more degraded (Figure 3E). IAV has been shown to degrade Pol II via interaction with its own polymerase selectively based on the phosphorylation status of the POLR2A.[153,154] At the same time, IAV also relies on Pol II for its replication, as the IAV RNA-dependent RNA polymerase (RdRP) binding to phosphorylated Pol II promotes the initiation of viral transcription and cap-snatching.[119] Nucleocytoplasmic transport machinery is another cellular entity required for the IAV life cycle. We found many tVAPs among components of the NPC stabilized by IAV infection, particularly of the NPC inner ring. The matrix protein M2, but not the components of the vRNP, was the only viral protein with cross-validated interaction with tVAPs in NPC (Figure 3D). IAV proteins also interact extensively with the nuclear import and export proteins. We found that the stability of importin α proteins was improved in IAV-infected cells, in line with the importance of importin α family members for IAV host adaptation as well as its genome replication.[87,155–157] By contrast, importin β family members also interact with IAV proteins but are mostly unchanged in their turnover rates (Figure 3D). The differential effects of viral protein binding on the stability of cellular proteins may reflect different involvement of these proteins in the virus life cycle. For instance, both KPNA6[94,98–100] and IPO5[94,97,99,100] were identified as IAV interactors by several studies. KPNA6 was strongly stabilized, and apart from its function in nuclear import, it was additionally found to form a complex with the viral ribonucleoprotein and the host factor ANP32 to maintain the activity of IAV RdRP.[157] However, the stability of IPO5 was not changed by IAV infection, and it was found to transiently transport the PB1-PA into the nucleus and is released from its interaction with PB1 by RanGTP inside the nucleus, allowing further binding of PB2 to the PB1-PA, forming the complete viral RdRP.[158]

tVAPs were enriched in host and restriction factors. When intersecting our data with published genome-wide screens, we found a highly significant enrichment of known host and restriction factors among the tVAPs with altered stability (Figure S4A; Table S4). Therefore, we hypothesized that the subset of tVAPs, which has not been associated with viral growth regulation, would contain many proteins relevant to IAV replication or restriction. Indeed, we discovered the pro- and antiviral functions of numerous tVAPs in loss-of-function analyses (Figure 4; Table S5). In particular, we identified CLIC4 and GPKOW as strong host and restriction factors, respectively. Notably, the additive effect of their turnover changes resulted in little change in the total abundance of these proteins in IAV infection, and their involvement in antiviral responses was only indicated by their turnover change (Figures 5A and S4E; Table S1). This demonstrates the importance of studying protein turnover to identify relevant virus-host relationships. CLIC4, a chloride channel found on cell surface and mitochondrial membranes, was identified as an interactor of IAV proteins[94] and a host factor for IAV in other studies.[98,116] Upon stress inducers like tumor necrosis factor alpha (TNF-α), DNA damage, or translation inhibition, it quickly translocates to the nucleus and promotes apoptosis.[159] It is tempting to speculate that IAV infection may induce the same translocation of CLIC4. Our study further focused on the

CellPress
OPEN ACCESS

role of GPKOW, a splicing factor[142,143] with an unknown role in virus infections so far. IAV hijacks and influences the host-splicing machinery to produce its own proteins and restricts the production of host antiviral factors,[120,122] and we identified many components of the host-splicing machinery as tVAPs (Figure 3F). It is, therefore, expected that many splicing factors are host factors for IAV.[120] However, the knockdown of GPKOW increased the reporter signals from IAV-Renilla and IAV-luciferase mini-replicon assays (Figures 4B, S4C, and S4F), and the same effect can be observed for other reporter viruses (Figure 5D). We found that this is likely due to the inhibited ISG response in cells with reduced GPKOW expression (Figures 5B, S5B, and S5E) and further pinpointed GPKOW's role upstream of IFN induction (Figures 5B, 5C, 5E, and S5E). The GPKOW homolog in plants, MOS2, contributes to plant innate immunity via the splicing of *SNC1*, a plant resistance protein, and the production of miRNA.[160,161] Therefore, GPKOW may act as a general guardian of cell homeostasis, and the effect of its disturbed function during virus infection may contribute to the immune response.[162]

In summary, our profiling of protein turnover during IAV infection revealed high functional relevance of the proteins with changing turnover, particularly degradation. We further demonstrated the potential effect of viral-host PPI on protein stability. Our study highlighted protein turnover as a previously underappreciated layer of virus-host interaction, from which the rich information will enable us to uncover host defense mechanisms and viral immune evasion strategies and thus facilitate the future development of antiviral therapies.

RESOURCE AVAILABILITY

Lead contact

Further information and requests for resources and reagents should be directed to and will be fulfilled by the lead contact, Andreas Pichlmair (andreas.pichlmair@tum.de).

Materials availability

This study did not generate new materials.

Data and code availability

- The mass spectrometry proteomics data have been deposited to the ProteomeXchange Consortium via the PRIDE[163] partner repository and are publicly available as of the date of publication. Accession numbers are listed in the key resources table. The data and analysis results are accessible online via the interactive web interface at pulsechase.innatelab.org.
- In-house R and Julia packages and scripts used for the bioinformatics analysis of the data have been deposited to public GitHub repositories: pcSILAC model and analysis scripts (https://doi.org/10.5281/zenodo.10231157); msglm (https://doi.org/10.5281/zenodo.7752068); msimportr (https://doi.org/10.5281/zenodo.7746897); OptEnrichSetCover (https://doi.org/10.5281/zenodo.4536596); analysis_utils_jl (package dependencies for the Julia packages and scripts used in this manuscript: https://doi.org/10.5281/zenodo.7752673).
- Any additional information required to reanalyze the data reported in this paper is available from the lead contact upon request.

ACKNOWLEDGMENTS

We would like to thank Susanne Maidl for technical support, Magdalena Zukowska for offering reagents, Melissa Verin for data management and visualization on the website, and M. Sabri Hamad for IT support. The work in the author's laboratory was funded by an ERC Consolidator grant (ERC-CoG ProDAP, 817798), the German Research Foundation (PI 1084/4, PI 1084/5, TRR179/TP10, TRR237/A07, and TRR353/B04), KA1-Co-02 "COVIPA" (Helmholtz Association's Initiative and Networking Fund), and the Center for Immunology of Viral Infections (CiViA) funded by the Danish National Research Foundation (DNRF 164).

AUTHOR CONTRIBUTIONS

Conceptualization, Y.H., C.U., P.H., A.S., and A.P.; methodology, P.H. and A.S.; formal analysis, Y.H., C.U., P.H., and A.S.; investigation, Y.H., C.U., and P.H.; writing – original draft, Y.H., A.S., and A.P.; writing – review & editing, Y.H., C.U., P.H., A.S., and A.P.; supervision, A.S. and A.P; funding acquisition, A.P.

DECLARATION OF INTERESTS

The authors declare no competing interests.

STAR★METHODS

Detailed methods are provided in the online version of this paper and include the following:

- KEY RESOURCES TABLE
- EXPERIMENTAL MODEL AND SUBJECT DETAILS
- METHOD DETAILS
  - IAV WSN mini replicon system
  - siRNA knockdown screen
  - CRISPR/Cas9 knockdown of GPKOW
  - Samples for proteomic analysis
  - IFN bioassay
  - Infection dynamics with live-imaging analysis
  - AHA-methionine pulse experiment
  - Integration of the published IAV datasets
- QUANTIFICATION AND STATISTICAL ANALYSIS
  - Sample preparation and data processing
  - Statistical analysis of MS data

SUPPLEMENTAL INFORMATION

Supplemental information can be found online at https://doi.org/10.1016/j.cels.2024.09.004.

Received: December 19, 2023
Revised: August 16, 2024
Accepted: September 13, 2024
Published: October 4, 2024

REFERENCES

1. Schwanhäusser, B., Busse, D., Li, N., Dittmar, G., Schuchhardt, J., Wolf, J., Chen, W., and Selbach, M. (2011). Global quantification of mammalian gene expression control. Nature *473*, 337–342. https://doi.org/10.1038/nature10098.
2. Maier, T., Güell, M., and Serrano, L. (2009). Correlation of mRNA and protein in complex biological samples. FEBS Lett. *583*, 3966–3973. https://doi.org/10.1016/j.febslet.2009.10.036.
3. Srivastava, H., Lippincott, M.J., Currie, J., Canfield, R., Lam, M.P.Y., and Lau, E. (2022). Protein prediction models support widespread post-transcriptional regulation of protein abundance by interacting partners. PLoS Comput. Biol. *18*, e1010702. https://doi.org/10.1371/journal.pcbi.1010702.
4. Lackner, D.H., Schmidt, M.W., Wu, S., Wolf, D.A., and Bähler, J. (2012). Regulation of transcriptome, translation, and proteome in response to

environmental stress in fission yeast. Genome Biol. *13*, R25. https://doi.org/10.1186/gb-2012-13-4-r25.

5. Lee, M.V., Topper, S.E., Hubler, S.L., Hose, J., Wenger, C.D., Coon, J.J., and Gasch, A.P. (2011). A dynamic model of proteome changes reveals new roles for transcript alteration in yeast. Mol. Syst. Biol. *7*, 514. https://doi.org/10.1038/msb.2011.48.
6. Jovanovic, M., Rooney, M.S., Mertins, P., Przybylski, D., Chevrier, N., Satija, R., Rodriguez, E.H., Fields, A.P., Schwartz, S., Raychowdhury, R., et al. (2015). Immunogenetics. Dynamic profiling of the protein life cycle in response to pathogens. Science *347*, 1259038. https://doi.org/10.1126/science.1259038.
7. Vogel, C., Silva, G.M., and Marcotte, E.M. (2011). Protein expression regulation under oxidative stress. Mol. Cell. Proteomics *10*, M111.009217. https://doi.org/10.1074/mcp.M111.009217.
8. Cheng, Z., Teo, G., Krueger, S., Rock, T.M., Koh, H.W.L., Choi, H., and Vogel, C. (2016). Differential dynamics of the mammalian mRNA and protein expression response to misfolding stress. Mol. Syst. Biol. *12*, 855. https://doi.org/10.15252/msb.20156423.
9. Nicolet, B.P., and Wolkers, M.C. (2022). The relationship of mRNA with protein expression in CD8+ T cells associates with gene class and gene characteristics. PLoS One *17*, e0276294. https://doi.org/10.1371/journal.pone.0276294.
10. Stern-Ginossar, N., Thompson, S.R., Mathews, M.B., and Mohr, I. (2019). Translational Control in Virus-Infected Cells. Cold Spring Harb. Perspect. Biol. *11*, a033001. https://doi.org/10.1101/cshperspect.a033001.
11. Liu, X., Hong, T., Parameswaran, S., Ernst, K., Marazzi, I., Weirauch, M.T., and Fuxman Bass, J.I. (2020). Human Virus Transcriptional Regulators. Cell *182*, 24–37. https://doi.org/10.1016/j.cell.2020.06.023.
12. Daly, R., Khaperskyy, D.A., and Gaglia, M.M. (2020). Fine-tuning a blunt tool: regulation of viral host shutoff RNases. PLoS Pathog. *16*, e1008385. https://doi.org/10.1371/journal.ppat.1008385.
13. Kawai, T., and Akira, S. (2006). Innate immune recognition of viral infection. Nat. Immunol. *7*, 131–137. https://doi.org/10.1038/ni1303.
14. Paludan, S.R., and Mogensen, T.H. (2022). Innate immunological pathways in COVID-19 pathogenesis. Sci. Immunol. *7*, eabm5505. https://doi.org/10.1126/sciimmunol.abm5505.
15. Zheng, J., Shi, W., Yang, Z., Chen, J., Qi, A., Yang, Y., Deng, Y., Yang, D., Song, N., Song, B., and Luo, D. (2023). RIG-I-like receptors: Molecular mechanism of activation and signaling. Adv. Immunol. *158*, 1–74. https://doi.org/10.1016/bs.ai.2023.03.001.
16. Iwasaki, A., and Pillai, P.S. (2014). Innate immunity to influenza virus infection. Nat. Rev. Immunol. *14*, 315–328. https://doi.org/10.1038/nri3665.
17. Iwasaki, A., and Medzhitov, R. (2015). Control of adaptive immunity by the innate immune system. Nat. Immunol. *16*, 343–353. https://doi.org/10.1038/ni.3123.
18. Colina, R., Costa-Mattioli, M., Dowling, R.J.O., Jaramillo, M., Tai, L.-H., Breitbach, C.J., Martineau, Y., Larsson, O., Rong, L., Svitkin, Y.V., et al. (2008). Translational control of the innate immune response through IRF-7. Nature *452*, 323–328. https://doi.org/10.1038/nature06730.
19. Ben-Asouli, Y., Banai, Y., Pel-Or, Y., Shir, A., and Kaempfer, R. (2002). Human interferon-gamma mRNA autoregulates its translation through a pseudoknot that activates the interferon-inducible protein kinase PKR. Cell *108*, 221–232. https://doi.org/10.1016/s0092-8674(02)00616-5.
20. Garcia-Sanz, J.A., and Lenig, D. (1996). Translational control of interleukin 2 messenger RNA as a molecular mechanism of T cell anergy. J. Exp. Med. *184*, 159–164. https://doi.org/10.1084/jem.184.1.159.
21. HamiltonII, B.J., NagyII, E., and RigbyoII, W.E.C. (1994). Enhanced Stability of Interleukin-2 mRNA in MIA 144 Cells. J. Biol. Chem. *269*, 5377–5383.
22. Goh, K.C., deVeer, M.J., and Williams, B.R. (2000). The protein kinase PKR is required for p38 MAPK activation and the innate immune response to bacterial endotoxin. EMBO J. *19*, 4292–4297. https://doi.org/10.1093/emboj/19.16.4292.
23. Gao, P., Liu, Y., Wang, H., Chai, Y., Weng, W., Zhang, Y., Zhou, L., Ge, X., Guo, X., Han, J., and Yang, H. (2022). Viral evasion of PKR restriction by reprogramming cellular stress granules. Proc. Natl. Acad. Sci. USA *119*, e2201169119. https://doi.org/10.1073/pnas.2201169119.
24. Zhang, S., Sun, Y., Chen, H., Dai, Y., Zhan, Y., Yu, S., Qiu, X., Tan, L., Song, C., and Ding, C. (2014). Activation of the PKR/eIF2α signaling cascade inhibits replication of Newcastle disease virus. Virol. J. *11*, 62. https://doi.org/10.1186/1743-422X-11-62.
25. Zuo, W., Wakimoto, M., Kozaiwa, N., Shirasaka, Y., Oh, S.-W., Fujiwara, S., Miyachi, H., Kogure, A., Kato, H., and Fujita, T. (2022). PKR and TLR3 trigger distinct signals that coordinate the induction of antiviral apoptosis. Cell Death Dis. *13*, 707. https://doi.org/10.1038/s41419-022-05101-3.
26. Schulz, O., Pichlmair, A., Rehwinkel, J., Rogers, N.C., Scheuner, D., Kato, H., Takeuchi, O., Akira, S., Kaufman, R.J., and Reis e Sousa, C. (2010). Protein kinase R contributes to immunity against specific viruses by regulating interferon mRNA integrity. Cell Host Microbe *7*, 354–361. https://doi.org/10.1016/j.chom.2010.04.007.
27. Peters, J.K., Tibble, R.W., Warminski, M., Jemielity, J., and Gross, J.D. (2022). Structure of the poxvirus decapping enzyme D9 reveals its mechanism of cap recognition and catalysis. Structure *30*, 721–732.e4. https://doi.org/10.1016/j.str.2022.02.012.
28. Parrish, S., Resch, W., and Moss, B. (2007). Vaccinia virus D10 protein has mRNA decapping activity, providing a mechanism for control of host and viral gene expression. Proc. Natl. Acad. Sci. USA *104*, 2139–2144. https://doi.org/10.1073/pnas.0611685104.
29. Schubert, K., Karousis, E.D., Jomaa, A., Scaiola, A., Echeverria, B., Gurzeler, L.-A., Leibundgut, M., Thiel, V., Mühlemann, O., and Ban, N. (2020). SARS-CoV-2 Nsp1 binds the ribosomal mRNA channel to inhibit translation. Nat. Struct. Mol. Biol. *27*, 959–966. https://doi.org/10.1038/s41594-020-0511-8.
30. Francisco-Velilla, R., Embarc-Buh, A., Abellan, S., and Martinez-Salas, E. (2022). Picornavirus translation strategies. FEBS Open Bio *12*, 1125–1141. https://doi.org/10.1002/2211-5463.13400.
31. Yang, X., Hu, Z., Fan, S., Zhang, Q., Zhong, Y., Guo, D., Qin, Y., and Chen, M. (2018). Picornavirus 2A protease regulates stress granule formation to facilitate viral translation. PLoS Pathog. *14*, e1006901. https://doi.org/10.1371/journal.ppat.1006901.
32. Nacken, W., Schreiber, A., Masemann, D., and Ludwig, S. (2021). The Effector Domain of the Influenza A Virus Nonstructural Protein NS1 Triggers Host Shutoff by Mediating Inhibition and Global Deregulation of Host Transcription When Associated with Specific Structures in the Nucleus. mBio *12*, e0219621. https://doi.org/10.1128/mBio.02196-21.
33. Ji, Z.-X., Wang, X.-Q., and Liu, X.-F. (2021). NS1: A Key Protein in the "Game" Between Influenza A Virus and Host in Innate Immunity. Front. Cell. Infect. Microbiol. *11*, 670177. https://doi.org/10.3389/fcimb.2021.670177.
34. Khaperskyy, D.A., Schmaling, S., Larkins-Ford, J., McCormick, C., and Gaglia, M.M. (2016). Selective Degradation of Host RNA Polymerase II Transcripts by Influenza A Virus PA-X Host Shutoff Protein. PLoS Pathog. *12*, e1005427. https://doi.org/10.1371/journal.ppat.1005427.
35. Chaimayo, C., Dunagan, M., Hayashi, T., Santoso, N., and Takimoto, T. (2018). Specificity and functional interplay between influenza virus PA-X and NS1 shutoff activity. PLoS Pathog. *14*, e1007465. https://doi.org/10.1371/journal.ppat.1007465.
36. Sha, T.W., Weber, M., Kasumba, D.M., Noda, T., Nakano, M., Kato, H., and Fujita, T. (2020). Influenza A virus NS1 optimises virus infectivity by enhancing genome packaging in a dsRNA-binding dependent manner. Virol. J. *17*, 107. https://doi.org/10.1186/s12985-020-01357-3.
37. Lipatov, A.S., Andreansky, S., Webby, R.J., Hulse, D.J., Rehg, J.E., Krauss, S., Perez, D.R., Doherty, P.C., Webster, R.G., and Sangster, M.Y. (2005). Pathogenesis of Hong Kong H5N1 influenza virus NS gene

reassortants in mice: the role of cytokines and B- and T-cell responses. J. Gen. Virol. *86*, 1121–1130. https://doi.org/10.1099/vir.0.80663-0.

38. Jiao, P., Tian, G., Li, Y., Deng, G., Jiang, Y., Liu, C., Liu, W., Bu, Z., Kawaoka, Y., and Chen, H. (2008). A single-amino-acid substitution in the NS1 protein changes the pathogenicity of H5N1 avian influenza viruses in mice. J. Virol. *82*, 1146–1154. https://doi.org/10.1128/JVI.01698-07.
39. Hu, J., Ma, C., and Liu, X. (2018). PA-X: a key regulator of influenza A virus pathogenicity and host immune responses. Med. Microbiol. Immunol. *207*, 255–269. https://doi.org/10.1007/s00430-018-0548-z.
40. Choi, Y., Bowman, J.W., and Jung, J.U. (2018). Autophagy during viral infection - a double-edged sword. Nat. Rev. Microbiol. *16*, 341–354. https://doi.org/10.1038/s41579-018-0003-6.
41. Miller, S., and Krijnse-Locker, J. (2008). Modification of intracellular membrane structures for virus replication. Nat. Rev. Microbiol. *6*, 363–374. https://doi.org/10.1038/nrmicro1890.
42. Imre, G. (2020). Cell death signalling in virus infection. Cell. Signal. *76*, 109772. https://doi.org/10.1016/j.cellsig.2020.109772.
43. Jevtić, P., Haakonsen, D.L., and Rapé, M. (2021). An E3 ligase guide to the galaxy of small-molecule-induced protein degradation. Cell Chem. Biol. *28*, 1000–1013. https://doi.org/10.1016/j.chembiol.2021.04.002.
44. Liu, T., Zhang, L., Joo, D., and Sun, S.-C. (2017). NF-κB signaling in inflammation. Signal Transduct. Target. Ther. *2*, 17023. https://doi.org/10.1038/sigtrans.2017.23.
45. Bellezza, I., Giambanco, I., Minelli, A., and Donato, R. (2018). Nrf2-Keap1 signaling in oxidative and reductive stress. Biochim. Biophys. Acta Mol. Cell Res. *1865*, 721–733. https://doi.org/10.1016/j.bbamcr.2018.02.010.
46. Herengt, A., Thyrsted, J., and Holm, C.K. (2021). NRF2 in Viral Infection. Antioxidants (Basel) *10*, 1491. https://doi.org/10.3390/antiox10091491.
47. Waqas, F.H., Shehata, M., Elgaher, W.A.M., Lacour, A., Kurmasheva, N., Begnini, F., Kiib, A.E., Dahlmann, J., Chen, C., Pavlou, A., et al. (2023). NRF2 activators inhibit influenza A virus replication by interfering with nucleo-cytoplasmic export of viral RNPs in an NRF2-independent manner. PLoS Pathog. *19*, e1011506. https://doi.org/10.1371/journal.ppat.1011506.
48. Perng, Y.-C., and Lenschow, D.J. (2018). ISG15 in antiviral immunity and beyond. Nat. Rev. Microbiol. *16*, 423–439. https://doi.org/10.1038/s41579-018-0020-5.
49. Villarroya-Beltri, C., Guerra, S., and Sánchez-Madrid, F. (2017). ISGylation - a key to lock the cell gates for preventing the spread of threats. J. Cell Sci. *130*, 2961–2969. https://doi.org/10.1242/jcs.205468.
50. Shi, H.-X., Yang, K., Liu, X., Liu, X.-Y., Wei, B., Shan, Y.-F., Zhu, L.-H., and Wang, C. (2010). Positive regulation of interferon regulatory factor 3 activation by Herc5 via ISG15 modification. Mol. Cell. Biol. *30*, 2424–2436. https://doi.org/10.1128/MCB.01466-09.
51. Chen, Z., Rijnbrand, R., Jangra, R.K., Devaraj, S.G., Qu, L., Ma, Y., Lemon, S.M., and Li, K. (2007). Ubiquitination and proteasomal degradation of interferon regulatory factor-3 induced by Npro from a cytopathic bovine viral diarrhea virus. Virology *366*, 277–292. https://doi.org/10.1016/j.virol.2007.04.023.
52. Bauhofer, O., Summerfield, A., Sakoda, Y., Tratschin, J.-D., Hofmann, M.A., and Ruggli, N. (2007). Classical swine fever virus Npro interacts with interferon regulatory factor 3 and induces its proteasomal degradation. J. Virol. *81*, 3087–3096. https://doi.org/10.1128/JVI.02032-06.
53. Luo, H. (2016). Interplay between the virus and the ubiquitin-proteasome system: molecular mechanism of viral pathogenesis. Curr. Opin. Virol. *17*, 1–10. https://doi.org/10.1016/j.coviro.2015.09.005.
54. Schneider, S.M., Lee, B.H., and Nicola, A.V. (2021). Viral entry and the ubiquitin-proteasome system. Cell. Microbiol. *23*, e13276. https://doi.org/10.1111/cmi.13276.
55. Boutell, C., Cuchet-Lourenço, D., Vanni, E., Orr, A., Glass, M., McFarlane, S., and Everett, R.D. (2011). A viral ubiquitin ligase has substrate preferential SUMO targeted ubiquitin ligase activity that counteracts intrinsic antiviral defence. PLoS Pathog. *7*, e1002245. https://doi.org/10.1371/journal.ppat.1002245.
56. Ulane, C.M., Kentsis, A., Cruz, C.D., Parisien, J.-P., Schneider, K.L., and Horvath, C.M. (2005). Composition and assembly of STAT-targeting ubiquitin ligase complexes: paramyxovirus V protein carboxyl terminus is an oligomerization domain. J. Virol. *79*, 10180–10189. https://doi.org/10.1128/JVI.79.16.10180-10189.2005.
57. Remoli, A.L., Marsili, G., Perrotti, E., Acchioni, C., Sgarbanti, M., Borsetti, A., Hiscott, J., and Battistini, A. (2016). HIV-1 Tat Recruits HDM2 E3 Ligase To Target IRF-1 for Ubiquitination and Proteasomal Degradation. mBio *7*, e01528-16. https://doi.org/10.1128/mBio.01528-16.
58. Zhou, D., Wang, Y., Tokunaga, K., Huang, F., Sun, B., and Yang, R. (2015). The HIV-1 accessory protein Vpr induces the degradation of the anti-HIV-1 agent APOBEC3G through a VprBP-mediated proteasomal pathway. Virus Res. *195*, 25–34. https://doi.org/10.1016/j.virusres.2014.08.021.
59. Douglas, J.L., Viswanathan, K., McCarroll, M.N., Gustin, J.K., Früh, K., and Moses, A.V. (2009). Vpu directs the degradation of the human immunodeficiency virus restriction factor BST-2/Tetherin via a {beta}TrCP-dependent mechanism. J. Virol. *83*, 7931–7947. https://doi.org/10.1128/JVI.00242-09.
60. Schwanhäusser, B., Gossen, M., Dittmar, G., and Selbach, M. (2009). Global analysis of cellular protein translation by pulsed SILAC. Proteomics *9*, 205–209. https://doi.org/10.1002/pmic.200800275.
61. Wolf, T., Jin, W., Zoppi, G., Vogel, I.A., Akhmedov, M., Bleck, C.K.E., Beltraminelli, T., Rieckmann, J.C., Ramirez, N.J., Benevento, M., et al. (2020). Dynamics in protein translation sustaining T cell preparedness. Nat. Immunol. *21*, 927–937. https://doi.org/10.1038/s41590-020-0714-5.
62. Bogenhagen, D.F., and Haley, J.D. (2020). Pulse-chase SILAC-based analyses reveal selective oversynthesis and rapid turnover of mitochondrial protein components of respiratory complexes. J. Biol. Chem. *295*, 2544–2554. https://doi.org/10.1074/jbc.RA119.011791.
63. McShane, E., Sin, C., Zauber, H., Wells, J.N., Donnelly, N., Wang, X., Hou, J., Chen, W., Storchova, Z., Marsh, J.A., et al. (2016). Kinetic Analysis of Protein Stability Reveals Age-Dependent Degradation. Cell *167*, 803–815.e21. https://doi.org/10.1016/j.cell.2016.09.015.
64. Bojkova, D., Klann, K., Koch, B., Widera, M., Krause, D., Ciesek, S., Cinatl, J., and Münch, C. (2020). Proteomics of SARS-CoV-2-infected host cells reveals therapy targets. Nature *583*, 469–472. https://doi.org/10.1038/s41586-020-2332-7.
65. Bogdanow, B., Wang, X., Eichelbaum, K., Sadewasser, A., Husic, I., Paki, K., Budt, M., Hergeselle, M., Vetter, B., Hou, J., et al. (2019). The dynamic proteome of influenza A virus infection identifies M segment splicing as a host range determinant. Nat. Commun. *10*, 5518. https://doi.org/10.1038/s41467-019-13520-8.
66. Nightingale, K., Lin, K.-M., Ravenhill, B.J., Davies, C., Nobre, L., Fielding, C.A., Ruckova, E., Fletcher-Etherington, A., Soday, L., Nichols, H., et al. (2018). High-Definition Analysis of Host Protein Stability during Human Cytomegalovirus Infection Reveals Antiviral Factors and Viral Evasion Mechanisms. Cell Host Microbe *24*, 447–460.e11. https://doi.org/10.1016/j.chom.2018.07.011.
67. Wu, C., Ba, Q., Lu, D., Li, W., Salovska, B., Hou, P., Mueller, T., Rosenberger, G., Gao, E., Di, Y., et al. (2021). Global and Site-Specific Effect of Phosphorylation on Protein Turnover. Dev. Cell *56*, 111–124.e6. https://doi.org/10.1016/j.devcel.2020.10.025.
68. Klann, K., Tascher, G., and Münch, C. (2020). Functional Translatome Proteomics Reveal Converging and Dose-Dependent Regulation by mTORC1 and eIF2α. Mol. Cell *77*, 913–925.e4. https://doi.org/10.1016/j.molcel.2019.11.010.
69. Bercovich-Kinori, A., Tai, J., Gelbart, I.A., Shitrit, A., Ben-Moshe, S., Drori, Y., Itzkovitz, S., Mandelboim, M., and Stern-Ginossar, N. (2016). A systematic view on influenza induced host shutoff. eLife *5*, e18311. https://doi.org/10.7554/eLife.18311.

70. Boisvert, F.-M., Ahmad, Y., Gierliński, M., Charrière, F., Lamont, D., Scott, M., Barton, G., and Lamond, A.I. (2012). A quantitative spatial proteomics analysis of proteome turnover in human cells. Mol. Cell. Proteomics *11*, M111.011429. https://doi.org/10.1074/mcp.M111.011429.

71. Zecha, J., Gabriel, W., Spallek, R., Chang, Y.-C., Mergner, J., Wilhelm, M., Bassermann, F., and Kuster, B. (2022). Linking post-translational modifications and protein turnover by site-resolved protein turnover profiling. Nat. Commun. *13*, 165. https://doi.org/10.1038/s41467-021-27639-0.

72. Schwanhäußer, B. (2011). Global analysis of cellular protein dynamics by pulse-labeling and quanti tati ve mass spectrometry. Preprint at Humboldt-Universität zu Berlin, Mathematisch-Naturwissenschaftliche Fakultät I. https://doi.org/10.18452/16305.

73. Greig, M.J., Niessen, S., Weinrich, S.L., Feng, J.L., Shi, M., and Johnson, T.O. (2015). Effects of Activating Mutations on EGFR Cellular Protein Turnover and Amino Acid Recycling Determined Using SILAC Mass Spectrometry. Int. J. Cell Biol. *2015*, 798936. https://doi.org/10.1155/2015/798936.

74. McInnes, L., Healy, J., Saul, N., and Großberger, L. (2018). UMAP: Uniform Manifold Approximation and Projection. J. Open Source Softw. *3*, 861. https://doi.org/10.21105/joss.00861.

75. Eisenreich, A., Bogdanov, V.Y., Zakrzewicz, A., Pries, A., Antoniak, S., Poller, W., Schultheiss, H.-P., and Rauch, U. (2009). Cdc2-like kinases and DNA topoisomerase I regulate alternative splicing of tissue factor in human endothelial cells. Circ. Res. *104*, 589–599. https://doi.org/10.1161/CIRCRESAHA.108.183905.

76. Fernbach, S., Spieler, E.E., Busnadiego, I., Karakus, U., Lkharrazi, A., Stertz, S., and Hale, B.G. (2022). Restriction factor screening identifies RABGAP1L-mediated disruption of endocytosis as a host antiviral defense. Cell Rep. *38*, 110549. https://doi.org/10.1016/j.celrep.2022.110549.

77. Becker, A.C., Gannagé, M., Giese, S., Hu, Z., Abou-Eid, S., Roubaty, C., Paul, P., Bühler, L., Gretzmeier, C., Dumit, V.I., et al. (2018). Influenza A Virus Induces Autophagosomal Targeting of Ribosomal Proteins. Mol. Cell. Proteomics *17*, 1909–1921. https://doi.org/10.1074/mcp.RA117.000364.

78. Smallwood, H.S., Duan, S., Morfouace, M., Rezinciuc, S., Shulkin, B.L., Shelat, A., Zink, E.E., Milasta, S., Bajracharya, R., Oluwaseum, A.J., et al. (2017). Targeting Metabolic Reprogramming by Influenza Infection for Therapeutic Intervention. Cell Rep. *19*, 1640–1653. https://doi.org/10.1016/j.celrep.2017.04.039.

79. Lin, S., Liu, N., Yang, Z., Song, W., Wang, P., Chen, H., Lucio, M., Schmitt-Kopplin, P., Chen, G., and Cai, Z. (2010). GC/MS-based metabolomics reveals fatty acid biosynthesis and cholesterol metabolism in cell lines infected with influenza A virus. Talanta *83*, 262–268. https://doi.org/10.1016/j.talanta.2010.09.019.

80. Tisoncik-Go, J., Gasper, D.J., Kyle, J.E., Eisfeld, A.J., Selinger, C., Hatta, M., Morrison, J., Korth, M.J., Zink, E.M., Kim, Y.-M., et al. (2016). Integrated Omics Analysis of Pathogenic Host Responses during Pandemic H1N1 Influenza Virus Infection: The Crucial Role of Lipid Metabolism. Cell Host Microbe *19*, 254–266. https://doi.org/10.1016/j.chom.2016.01.002.

81. Blanc, M., Hsieh, W.Y., Robertson, K.A., Watterson, S., Shui, G., Lacaze, P., Khondoker, M., Dickinson, P., Sing, G., Rodríguez-Martín, S., et al. (2011). Host defense against viral infection involves interferon mediated down-regulation of sterol biosynthesis. PLoS Biol. *9*, e1000598. https://doi.org/10.1371/journal.pbio.1000598.

82. Mazel-Sanchez, B., Iwaszkiewicz, J., Bonifacio, J.P.P., Silva, F., Niu, C., Strohmeier, S., Eletto, D., Krammer, F., Tan, G., Zoete, V., et al. (2021). Influenza A viruses balance ER stress with host protein synthesis shutoff. Proc. Natl. Acad. Sci. USA *118*, e2024681118. https://doi.org/10.1073/pnas.2024681118.

83. Martín-Vicente, M., Medrano, L.M., Resino, S., García-Sastre, A., and Martínez, I. (2017). TRIM25 in the Regulation of the Antiviral Innate Immunity. Front. Immunol. *8*, 1187. https://doi.org/10.3389/fimmu.2017.01187.

84. Bonaventure, B., and Goujon, C. (2022). DExH/D-box helicases at the frontline of intrinsic and innate immunity against viral infections. J. Gen. Virol. *103*. https://doi.org/10.1099/jgv.0.001766.

85. Gabriel, G., Herwig, A., and Klenk, H.-D. (2008). Interaction of polymerase subunit PB2 and NP with importin alpha1 is a determinant of host range of influenza A virus. PLoS Pathog. *4*, e11. https://doi.org/10.1371/journal.ppat.0040011.

86. Resa-Infante, P., Jorba, N., Zamarreño, N., Fernández, Y., Juárez, S., and Ortín, J. (2008). The host-dependent interaction of alpha-importins with influenza PB2 polymerase subunit is required for virus RNA replication. PLoS One *3*, e3904. https://doi.org/10.1371/journal.pone.0003904.

87. Gabriel, G., Klingel, K., Otte, A., Thiele, S., Hudjetz, B., Arman-Kalcek, G., Sauter, M., Shmidt, T., Rother, F., Baumgarte, S., et al. (2011). Differential use of importin-α isoforms governs cell tropism and host adaptation of influenza virus. Nat. Commun. *2*, 156. https://doi.org/10.1038/ncomms1158.

88. Thai, M., Thaker, S.K., Feng, J., Du, Y., Hu, H., Ting Wu, T., Graeber, T.G., Braas, D., and Christofk, H.R. (2015). MYC-induced reprogramming of glutamine catabolism supports optimal virus replication. Nat. Commun. *6*, 8873. https://doi.org/10.1038/ncomms9873.

89. Kawaguchi, A., and Nagata, K. (2007). De novo replication of the influenza virus RNA genome is regulated by DNA replicative helicase, MCM. EMBO J. *26*, 4566–4575. https://doi.org/10.1038/sj.emboj.7601881.

90. Gack, M.U., Albrecht, R.A., Urano, T., Inn, K.-S., Huang, I.-C., Carnero, E., Farzan, M., Inoue, S., Jung, J.U., and García-Sastre, A. (2009). Influenza A virus NS1 targets the ubiquitin ligase TRIM25 to evade recognition by the host viral RNA sensor RIG-I. Cell Host Microbe *5*, 439–449. https://doi.org/10.1016/j.chom.2009.04.006.

91. Hale, B.G., Randall, R.E., Ortín, J., and Jackson, D. (2008). The multifunctional NS1 protein of influenza A viruses. J. Gen. Virol. *89*, 2359–2376. https://doi.org/10.1099/vir.0.2008/004606-0.

92. Avanthay, R., Garcia-Nicolas, O., Zimmer, G., and Summerfield, A. (2023). NS1 and PA-X of H1N1/09 influenza virus act in a concerted manner to manipulate the innate immune response of porcine respiratory epithelial cells. Front. Cell. Infect. Microbiol. *13*, 1222805. https://doi.org/10.3389/fcimb.2023.1222805.

93. Griss, J., Viteri, G., Sidiropoulos, K., Nguyen, V., Fabregat, A., and Hermjakob, H. (2020). ReactomeGSA - Efficient Multi-Omics Comparative Pathway Analysis. Mol. Cell. Proteomics *19*, 2115–2125. https://doi.org/10.1074/mcp.TIR120.002155.

94. Watanabe, T., Kawakami, E., Shoemaker, J.E., Lopes, T.J.S., Matsuoka, Y., Tomita, Y., Kozuka-Hata, H., Gorai, T., Kuwahara, T., Takeda, E., et al. (2014). Influenza virus-host interactome screen as a platform for antiviral drug development. Cell Host Microbe *16*, 795–805. https://doi.org/10.1016/j.chom.2014.11.002.

95. Sun, M.-S., Zhang, J., Jiang, L.-Q., Pan, Y.-X., Tan, J.-Y., Yu, F., Guo, L., Yin, L., Shen, C., Shu, H.-B., and Liu, Y. (2018). TMED2 Potentiates Cellular IFN Responses to DNA Viruses by Reinforcing MITA Dimerization and Facilitating Its Trafficking. Cell Rep. *25*, 3086–3098.e3. https://doi.org/10.1016/j.celrep.2018.11.048.

96. Holm, C.K., Rahbek, S.H., Gad, H.H., Bak, R.O., Jakobsen, M.R., Jiang, Z., Hansen, A.L., Jensen, S.K., Sun, C., Thomsen, M.K., et al. (2016). Influenza A virus targets a cGAS-independent STING pathway that controls enveloped RNA viruses. Nat. Commun. *7*, 10680. https://doi.org/10.1038/ncomms10680.

97. Heaton, N.S., Moshkina, N., Fenouil, R., Gardner, T.J., Aguirre, S., Shah, P.S., Zhao, N., Manganaro, L., Hultquist, J.F., Noel, J., et al. (2016). Targeting Viral Proteostasis Limits Influenza Virus, HIV, and Dengue Virus Infection. Immunity *44*, 46–58. https://doi.org/10.1016/j.immuni.2015.12.017.

98. Shapira, S.D., Gat-Viks, I., Shum, B.O.V., Dricot, A., de Grace, M.M., Wu, L., Gupta, P.B., Hao, T., Silver, S.J., Root, D.E., et al. (2009). A physical

and regulatory map of host-influenza interactions reveals pathways in H1N1 infection. Cell *139*, 1255–1267. https://doi.org/10.1016/j.cell.2009.12.018.

99. Tripathi, S., Pohl, M.O., Zhou, Y., Rodriguez-Frandsen, A., Wang, G., Stein, D.A., Moulton, H.M., DeJesus, P., Che, J., Mulder, L.C.F., et al. (2015). Meta- and Orthogonal Integration of Influenza "OMICs" Data Defines a Role for UBR4 in Virus Budding. Cell Host Microbe *18*, 723–735. https://doi.org/10.1016/j.chom.2015.11.002.

100. Wang, L., Fu, B., Li, W., Patil, G., Liu, L., Dorf, M.E., and Li, S. (2017). Comparative influenza protein interactomes identify the role of plakophilin 2 in virus restriction. Nat. Commun. *8*, 13876. https://doi.org/10.1038/ncomms13876.

101. He, Y., Xu, K., Keiner, B., Zhou, J., Czudai, V., Li, T., Chen, Z., Liu, J., Klenk, H.-D., Shu, Y.L., and Sun, B. (2010). Influenza A virus replication induces cell cycle arrest in G0/G1 phase. J. Virol. *84*, 12832–12840. https://doi.org/10.1128/JVI.01216-10.

102. Jiang, W., Wang, Q., Chen, S., Gao, S., Song, L., Liu, P., and Huang, W. (2013). Influenza A virus NS1 induces G0/G1 cell cycle arrest by inhibiting the expression and activity of RhoA protein. J. Virol. *87*, 3039–3052. https://doi.org/10.1128/JVI.03176-12.

103. Smogorzewska, A., Matsuoka, S., Vinciguerra, P., McDonald, E.R., 3rd, Hurov, K.E., Luo, J., Ballif, B.A., Gygi, S.P., Hofmann, K., D'Andrea, A.D., and Elledge, S.J. (2007). Identification of the FANCI protein, a monoubiquitinated FANCD2 paralog required for DNA repair. Cell *129*, 289–301. https://doi.org/10.1016/j.cell.2007.03.009.

104. Huang, J., Gong, Z., Ghosal, G., and Chen, J. (2009). SOSS complexes participate in the maintenance of genomic stability. Mol. Cell *35*, 384–393. https://doi.org/10.1016/j.molcel.2009.06.011.

105. Liu, L., Chen, H., Chen, X., Yao, C., Shen, W., and Jia, C. (2023). KNTC1 as a putative tumor oncogene in pancreatic cancer. J. Cancer Res. Clin. Oncol. *149*, 3023–3031. https://doi.org/10.1007/s00432-022-04146-3.

106. Jin, L., Williamson, A., Banerjee, S., Philipp, I., and Rape, M. (2008). Mechanism of ubiquitin-chain formation by the human anaphase-promoting complex. Cell *133*, 653–665. https://doi.org/10.1016/j.cell.2008.04.012.

107. Chatterjee, S., Naidu, G.S., Hazan-Halevy, I., Grobe, H., Ezra, A., Sharma, P., Goldsmith, M., Ramishetti, S., Sprinzak, D., Zaidel-Bar, R., and Peer, D. (2023). Therapeutic gene silencing of CKAP5 leads to lethality in genetically unstable cancer cells. Sci. Adv. *9*, eade4800. https://doi.org/10.1126/sciadv.ade4800.

108. Cai, X., Gao, J., Shi, C., Guo, W.Z., Guo, D., and Zhang, S. (2022). The role of NCAPG in various of tumors. Biomed. Pharmacother. *155*, 113635. https://doi.org/10.1016/j.biopha.2022.113635.

109. Kimura, K., Cuvier, O., and Hirano, T. (2001). Chromosome condensation by a human condensin complex in Xenopus egg extracts. J. Biol. Chem. *276*, 5417–5420. https://doi.org/10.1074/jbc.C000873200.

110. Uusküla-Reimand, L., and Wilson, M.D. (2022). Untangling the roles of TOP2A and TOP2B in transcription and cancer. Sci. Adv. *8*, eadd4920. https://doi.org/10.1126/sciadv.add4920.

111. Xie, X., Wang, Z., and Chen, Y. (2007). Association of LKB1 with a WD-repeat protein WDR6 is implicated in cell growth arrest and p27(Kip1) induction. Mol. Cell. Biochem. *301*, 115–122. https://doi.org/10.1007/s11010-006-9402-5.

112. Chung, H.K., Yi, Y.-W., Jung, N.-C., Kim, D., Suh, J.M., Kim, H., Park, K.C., Song, J.H., Kim, D.W., Hwang, E.S., et al. (2003). CR6-interacting factor 1 interacts with Gadd45 family proteins and modulates the cell cycle. J. Biol. Chem. *278*, 28079–28088. https://doi.org/10.1074/jbc.M212835200.

113. Soudani, N., Hage-Sleiman, R., Karam, W., Dbaibo, G., and Zaraket, H. (2019). Ceramide Suppresses Influenza A Virus Replication In Vitro. J. Virol. *93*, e00053-19. https://doi.org/10.1128/JVI.00053-19.

114. Haugstetter, J., Blicher, T., and Ellgaard, L. (2005). Identification and characterization of a novel thioredoxin-related transmembrane protein of the endoplasmic reticulum. J. Biol. Chem. *280*, 8371–8380. https://doi.org/10.1074/jbc.M413924200.

115. Betakova, T., and Hay, A.J. (2009). Stability and function of the influenza A virus M2 ion channel protein is determined by both extracellular and cytoplasmic domains. Arch. Virol. *154*, 147–151. https://doi.org/10.1007/s00705-008-0283-7.

116. Karlas, A., Machuy, N., Shin, Y., Pleissner, K.-P., Artarini, A., Heuer, D., Becker, D., Khalil, H., Ogilvie, L.A., Hess, S., et al. (2010). Genome-wide RNAi screen identifies human host factors crucial for influenza virus replication. Nature *463*, 818–822. https://doi.org/10.1038/nature08760.

117. Pashkov, E.A., Faizuloev, E.B., Korchevaya, E.R., Rtishchev, A.A., Cherepovich, B.S., Sidorov, A.V., Poddubikov, A.V., Bystritskaya, E.P., Dronina, Y.E., Bykov, A.S., et al. (2022). Knockdown of *FLT4*, *Nup98*, and *Nup205* cellular genes as a suppressor for the viral activity of Influenza A/WSN/33 (H1N1) in A549 cell culture. Тонкие химические технологии *16*, 476–489.

118. York, A., Hutchinson, E.C., and Fodor, E. (2014). Interactome analysis of the influenza A virus transcription/replication machinery identifies protein phosphatase 6 as a cellular factor required for efficient virus replication. J. Virol. *88*, 13284–13299. https://doi.org/10.1128/JVI.01813-14.

119. Walker, A.P., and Fodor, E. (2019). Interplay between Influenza Virus and the Host RNA Polymerase II Transcriptional Machinery. Trends Microbiol. *27*, 398–407. https://doi.org/10.1016/j.tim.2018.12.013.

120. Dubois, J., Terrier, O., and Rosa-Calatrava, M. (2014). Influenza viruses and mRNA splicing: doing more with less. mBio *5*, e00070. https://doi.org/10.1128/mBio.00070-14.

121. Ashraf, U., Benoit-Pilven, C., Navratil, V., Ligneau, C., Fournier, G., Munier, S., Sismeiro, O., Coppée, J.-Y., Lacroix, V., and Naffakh, N. (2020). Influenza virus infection induces widespread alterations of host cell splicing. NAR Genom. Bioinform. *2*, lqaa095. https://doi.org/10.1093/nargab/lqaa095.

122. Thompson, M.G., Dittmar, M., Mallory, M.J., Bhat, P., Ferretti, M.B., Fontoura, B.M., Cherry, S., and Lynch, K.W. (2020). Viral-induced alternative splicing of host genes promotes influenza replication. eLife *9*, e55500. https://doi.org/10.7554/eLife.55500.

123. Shao, W., Kim, H.-S., Cao, Y., Xu, Y.-Z., and Query, C.C. (2012). A U1-U2 snRNP interaction network during intron definition. Mol. Cell. Biol. *32*, 470–478. https://doi.org/10.1128/MCB.06234-11.

124. Gu, W., Gallagher, G.R., Dai, W., Liu, P., Li, R., Trombly, M.I., Gammon, D.B., Mello, C.C., Wang, J.P., and Finberg, R.W. (2015). Influenza A virus preferentially snatches noncoding RNA caps. RNA *21*, 2067–2075. https://doi.org/10.1261/rna.054221.115.

125. Li, Q., Jiang, Z., Ren, S., Guo, H., Song, Z., Chen, S., Gao, X., Meng, F., Zhu, J., Liu, L., et al. (2022). SRSF5-Mediated Alternative Splicing of M Gene is Essential for Influenza A Virus Replication: A Host-Directed Target Against Influenza Virus. Adv. Sci. (Weinh) *9*, e2203088. https://doi.org/10.1002/advs.202203088.

126. Brass, A.L., Huang, I.-C., Benita, Y., John, S.P., Krishnan, M.N., Feeley, E.M., Ryan, B.J., Weyer, J.L., van der Weyden, L., Fikrig, E., et al. (2009). The IFITM proteins mediate cellular resistance to influenza A H1N1 virus, West Nile virus, and dengue virus. Cell *139*, 1243–1254. https://doi.org/10.1016/j.cell.2009.12.017.

127. König, R., Stertz, S., Zhou, Y., Inoue, A., Hoffmann, H.-H., Bhattacharyya, S., Alamares, J.G., Tscherne, D.M., Ortigoza, M.B., Liang, Y., et al. (2010). Human host factors required for influenza virus replication. Nature *463*, 813–817. https://doi.org/10.1038/nature08699.

128. Ward, S.E., Kim, H.S., Komurov, K., Mendiratta, S., Tsai, P.-L., Schmolke, M., Satterly, N., Manicassamy, B., Forst, C.V., Roth, M.G., et al. (2012). Host modulators of H1N1 cytopathogenicity. PLoS One *7*, e39284.

129. Song, Y., Huang, H., Hu, Y., Zhang, J., Li, F., Yin, X., Shi, J., Li, Y., Li, C., Zhao, D., and Chen, H. (2021). A genome-wide CRISPR/Cas9 gene knockout screen identifies immunoglobulin superfamily DCC subclass member 4 as a key host factor that promotes influenza virus endocytosis.

PLoS Pathog. *17*, e1010141. https://doi.org/10.1371/journal.ppat.1010141.

130. Yi, C., Cai, C., Cheng, Z., Zhao, Y., Yang, X., Wu, Y., Wang, X., Jin, Z., Xiang, Y., Jin, M., et al. (2022). Genome-wide CRISPR-Cas9 screening identifies the CYTH2 host gene as a potential therapeutic target of influenza viral infection. Cell Rep. *38*, 110559. https://doi.org/10.1016/j.celrep.2022.110559.

131. Li, B., Clohisey, S.M., Chia, B.S., Wang, B., Cui, A., Eisenhaure, T., Schweitzer, L.D., Hoover, P., Parkinson, N.J., Nachshon, A., et al. (2020). Genome-wide CRISPR screen identifies host dependency factors for influenza A virus infection. Nat. Commun. *11*, 164. https://doi.org/10.1038/s41467-019-13965-x.

132. Han, J., Perez, J.T., Chen, C., Li, Y., Benitez, A., Kandasamy, M., Lee, Y., Andrade, J., tenOever, B., and Manicassamy, B. (2018). Genome-wide CRISPR/Cas9 Screen Identifies Host Factors Essential for Influenza Virus Replication. Cell Rep. *23*, 596–607. https://doi.org/10.1016/j.celrep.2018.03.045.

133. Sharon, D.M., Nesdoly, S., Yang, H.J., Gélinas, J.-F., Xia, Y., Ansorge, S., and Kamen, A.A. (2020). A pooled genome-wide screening strategy to identify and rank influenza host restriction factors in cell-based vaccine production platforms. Sci. Rep. *10*, 12166. https://doi.org/10.1038/s41598-020-68934-y.

134. Heaton, B.E., Kennedy, E.M., Dumm, R.E., Harding, A.T., Sacco, M.T., Sachs, D., and Heaton, N.S. (2017). A CRISPR Activation Screen Identifies a Pan-avian Influenza Virus Inhibitory Host Factor. Cell Rep *20*, 1503–1512. https://doi.org/10.1016/j.celrep.2017.07.060.

135. Du, Y., Yang, F., Wang, Q., Xu, N., Xie, Y., Chen, S., Qin, T., and Peng, D. (2020). Influenza a virus antagonizes type I and type II interferon responses via SOCS1-dependent ubiquitination and degradation of JAK1. Virol. J. *17*, 74. https://doi.org/10.1186/s12985-020-01348-4.

136. Yi, C., Zhao, Z., Wang, S., Sun, X., Zhang, D., Sun, X., Zhang, A., and Jin, M. (2017). Influenza A Virus PA Antagonizes Interferon-β by Interacting with Interferon Regulatory Factor 3. Front. Immunol. *8*, 1051. https://doi.org/10.3389/fimmu.2017.01051.

137. Wang, X., Wu, Z., Li, Y., Yang, Y., Xiao, C., Liu, X., Xiang, X., Wei, J., Shao, D., Liu, K., et al. (2020). p53 promotes ZDHHC1-mediated IFITM3 palmitoylation to inhibit Japanese encephalitis virus replication. PLoS Pathog. *16*, e1009035. https://doi.org/10.1371/journal.ppat.1009035.

138. Bateman, A.C., Karamanska, R., Busch, M.G., Dell, A., Olsen, C.W., and Haslam, S.M. (2010). Glycan analysis and influenza A virus infection of primary swine respiratory epithelial cells: the importance of NeuAc {alpha}2-6 glycans. J. Biol. Chem. *285*, 34016–34026. https://doi.org/10.1074/jbc.M110.115998.

139. Müller, K.H., Kainov, D.E., El Bakkouri, K., Saelens, X., De Brabander, J.K., Kittel, C., Samm, E., and Muller, C.P. (2011). The proton translocation domain of cellular vacuolar ATPase provides a target for the treatment of influenza A virus infections. Br. J. Pharmacol. *164*, 344–357. https://doi.org/10.1111/j.1476-5381.2011.01346.x.

140. Hubel, P., Urban, C., Bergant, V., Schneider, W.M., Knauer, B., Stukalov, A., Scaturro, P., Mann, A., Brunotte, L., Hoffmann, H.H., et al. (2019). A protein-interaction network of interferon-stimulated genes extends the innate immune system landscape. Nat. Immunol. *20*, 493–502. https://doi.org/10.1038/s41590-019-0323-3.

141. Yang, H., Dong, Y., Bian, Y., Xu, N., Wu, Y., Yang, F., Du, Y., Qin, T., Chen, S., Peng, D., and Liu, X. (2022). The influenza virus PB2 protein evades antiviral innate immunity by inhibiting JAK1/STAT signalling. Nat. Commun. *13*, 6288. https://doi.org/10.1038/s41467-022-33909-2.

142. Hegele, A., Kamburov, A., Grossmann, A., Sourlis, C., Wowro, S., Weimann, M., Will, C.L., Pena, V., Lührmann, R., and Stelzl, U. (2012). Dynamic protein-protein interaction wiring of the human spliceosome. Mol. Cell *45*, 567–580. https://doi.org/10.1016/j.molcel.2011.12.034.

143. Zang, S., Lin, T.-Y., Chen, X., Gencheva, M., Newo, A.N.S., Yang, L., Rossi, D., Hu, J., Lin, S.-B., Huang, A., and Lin, R.J. (2014). GPKOW is essential for pre-mRNA splicing in vitro and suppresses splicing defect caused by dominant-negative DHX16 mutation in vivo. Biosci. Rep. *34*, e00163. https://doi.org/10.1042/BSR20140142.

144. de Rozières, C.M., Pequeno, A., Shahabi, S., Lucas, T.M., Godula, K., Ghosh, G., and Joseph, S. (2022). PABP1 Drives the Selective Translation of Influenza A Virus mRNA. J. Mol. Biol. *434*, 167460. https://doi.org/10.1016/j.jmb.2022.167460.

145. Tran, V., Ledwith, M.P., Thamamongood, T., Higgins, C.A., Tripathi, S., Chang, M.W., Benner, C., García-Sastre, A., Schwemmle, M., Boon, A.C.M., et al. (2020). Influenza virus repurposes the antiviral protein IFIT2 to promote translation of viral mRNAs. Nat. Microbiol. *5*, 1490–1503. https://doi.org/10.1038/s41564-020-0778-x.

146. Ayari, A., Rosa-Calatrava, M., Lancel, S., Barthelemy, J., Pizzorno, A., Mayeuf-Louchart, A., Baron, M., Hot, D., Deruyter, L., Soulard, D., et al. (2020). Influenza infection rewires energy metabolism and induces browning features in adipose cells and tissues. Commun. Biol. *3*, 237. https://doi.org/10.1038/s42003-020-0965-6.

147. Chen, K.-K., Minakuchi, M., Wuputra, K., Ku, C.-C., Pan, J.-B., Kuo, K.-K., Lin, Y.-C., Saito, S., Lin, C.-S., and Yokoyama, K.K. (2020). Redox control in the pathophysiology of influenza virus infection. BMC Microbiol. *20*, 214. https://doi.org/10.1186/s12866-020-01890-9.

148. Ren, L., Zhang, W., Zhang, J., Zhang, J., Zhang, H., Zhu, Y., Meng, X., Yi, Z., and Wang, R. (2021). Influenza A Virus (H1N1) Infection Induces Glycolysis to Facilitate Viral Replication. Virol. Sin. *36*, 1532–1542. https://doi.org/10.1007/s12250-021-00433-4.

149. Soto, I., Couvillion, M., Hansen, K.G., McShane, E., Moran, J.C., Barrientos, A., and Churchman, L.S. (2022). Balanced mitochondrial and cytosolic translatomes underlie the biogenesis of human respiratory complexes. Genome Biol. *23*, 170. https://doi.org/10.1186/s13059-022-02732-9.

150. Pohl, C., and Dikic, I. (2019). Cellular quality control by the ubiquitin-proteasome system and autophagy. Science *366*, 818–822. https://doi.org/10.1126/science.aax3769.

151. Murata, S., Takahama, Y., Kasahara, M., and Tanaka, K. (2018). The immunoproteasome and thymoproteasome: functions, evolution and human disease. Nat. Immunol. *19*, 923–931. https://doi.org/10.1038/s41590-018-0186-z.

152. Yang, C.-H., Hsu, C.-F., Lai, X.-Q., Chan, Y.-R., Li, H.-C., and Lo, S.-Y. (2022). Cellular PSMB4 Protein Suppresses Influenza A Virus Replication through Targeting NS1 Protein. Viruses *14*, 2277. https://doi.org/10.3390/v14102277.

153. Rodriguez, A., Pérez-González, A., and Nieto, A. (2007). Influenza virus infection causes specific degradation of the largest subunit of cellular RNA polymerase II. J. Virol. *81*, 5315–5324. https://doi.org/10.1128/JVI.02129-06.

154. Vreede, F.T., Chan, A.Y., Sharps, J., and Fodor, E. (2010). Mechanisms and functional implications of the degradation of host RNA polymerase II in influenza virus infected cells. Virology *396*, 125–134. https://doi.org/10.1016/j.virol.2009.10.003.

155. Pumroy, R.A., Ke, S., Hart, D.J., Zachariae, U., and Cingolani, G. (2015). Molecular determinants for nuclear import of influenza A PB2 by importin α isoforms 3 and 7. Structure *23*, 374–384. https://doi.org/10.1016/j.str.2014.11.015.

156. Resa-Infante, P., Thieme, R., Ernst, T., Arck, P.C., Ittrich, H., Reimer, R., and Gabriel, G. (2014). Importin-α7 is required for enhanced influenza A virus replication in the alveolar epithelium and severe lung damage in mice. J. Virol. *88*, 8166–8179. https://doi.org/10.1128/JVI.00270-14.

157. Yu, M., Sun, L., Zhang, Z., Zhang, Y., Zhang, H., Na, L., and Wang, X. (2022). KPNA6 is a Cofactor of ANP32A/B in Supporting Influenza Virus Polymerase Activity. Microbiol. Spectr. *10*, e0207321. https://doi.org/10.1128/spectrum.02073-21.

158. Deng, T., Engelhardt, O.G., Thomas, B., Akoulitchev, A.V., Brownlee, G.G., and Fodor, E. (2006). Role of ran binding protein 5 in nuclear import and assembly of the influenza virus RNA polymerase complex. J. Virol. *80*, 11911–11919. https://doi.org/10.1128/JVI.01565-06.

159. Suh, K.S., Mutoh, M., Nagashima, K., Fernandez-Salas, E., Edwards, L.E., Hayes, D.D., Crutchley, J.M., Marin, K.G., Dumont, R.A., Levy, J.M., et al. (2004). The Organellular Chloride Channel Protein CLIC4/mtCLIC Translocates to the Nucleus in Response to Cellular Stress and Accelerates Apoptosis*. J. Biol. Chem. *279*, 4632–4641. https://doi.org/10.1074/jbc.M311632200.

160. Zhang, Y., Cheng, Y.T., Bi, D., Palma, K., and Li, X. (2005). MOS2, a protein containing G-patch and KOW motifs, is essential for innate immunity in Arabidopsis thaliana. Curr. Biol. *15*, 1936–1942. https://doi.org/10.1016/j.cub.2005.09.038.

161. Copeland, C., Xu, S., Qi, Y., and Li, X. (2013). MOS2 has redundant function with its homolog MOS2H and is required for proper splicing of SNC1. Plant Signal. Behav. *8*. https://doi.org/10.4161/psb.25372.

162. Remick, B.C., Gaidt, M.M., and Vance, R.E. (2023). Effector-Triggered Immunity. Annu. Rev. Immunol. *41*, 453–481. https://doi.org/10.1146/annurev-immunol-101721-031732.

163. Perez-Riverol, Y., Bai, J., Bandla, C., García-Seisdedos, D., Hewapathirana, S., Kamatchinathan, S., Kundu, D.J., Prakash, A., Frericks-Zipper, A., Eisenacher, M., et al. (2022). The PRIDE database resources in 2022: a hub for mass spectrometry-based proteomics evidences. Nucleic Acids Res. *50*, D543–D552. https://doi.org/10.1093/nar/gkab1038.

164. Kochs, G., Koerner, I., Thiel, L., Kothlow, S., Kaspers, B., Ruggli, N., Summerfield, A., Pavlovic, J., Stech, J., and Staeheli, P. (2007). Properties of H7N7 influenza A virus strain SC35M lacking interferon antagonist NS1 in mice and chickens. J. Gen. Virol. *88*, 1403–1409. https://doi.org/10.1099/vir.0.82764-0.

165. Reuther, P., Göpfert, K., Dudek, A.H., Heiner, M., Herold, S., and Schwemmle, M. (2015). Generation of a variety of stable Influenza A reporter viruses by genetic engineering of the NS gene segment. Sci. Rep. *5*, 11346. https://doi.org/10.1038/srep11346.

166. Haas, D.A., Meiler, A., Geiger, K., Vogt, C., Preuss, E., Kochs, G., and Pichlmair, A. (2018). Viral targeting of TFIIB impairs de novo polymerase II recruitment and affects antiviral immunity. PLoS Pathog. *14*, e1006980. https://doi.org/10.1371/journal.ppat.1006980.

167. Goldeck, M., Schlee, M., Hartmann, G., and Hornung, V. (2014). Enzymatic Synthesis and Purification of a Defined RIG-I Ligand. In Innate DNA and RNA Recognition: Methods and Protocols, H.-J. Anders and A. Migliorini, eds. (Springer), pp. 15–25. https://doi.org/10.1007/978-1-4939-0882-0_2.

168. Dittmann, J., Stertz, S., Grimm, D., Steel, J., García-Sastre, A., Haller, O., and Kochs, G. (2008). Influenza A virus strains differ in sensitivity to the antiviral action of Mx-GTPase. J. Virol. *82*, 3624–3631. https://doi.org/10.1128/JVI.01753-07.

169. Tyanova, S., Temu, T., and Cox, J. (2016). The MaxQuant computational platform for mass spectrometry-based shotgun proteomics. Nat. Protoc. *11*, 2301–2319. https://doi.org/10.1038/nprot.2016.136.

170. Shannon, P., Markiel, A., Ozier, O., Baliga, N.S., Wang, J.T., Ramage, D., Amin, N., Schwikowski, B., and Ideker, T. (2003). Cytoscape: a software environment for integrated models of biomolecular interaction networks. Genome Res. *13*, 2498–2504. https://doi.org/10.1101/gr.1239303.

171. Holze, C., Michaudel, C., Mackowiak, C., Haas, D.A., Benda, C., Hubel, P., Pennemann, F.L., Schnepf, D., Wettmarshausen, J., Braun, M., et al. (2018). Oxeiptosis, a ROS-induced caspase-independent apoptosis-like cell-death pathway. Nat. Immunol. *19*, 130–140. https://doi.org/10.1038/s41590-017-0013-y.

172. Laudenbach, B.T., Krey, K., Emslander, Q., Andersen, L.L., Reim, A., Scaturro, P., Mundigl, S., Dächert, C., Manske, K., Moser, M., et al. (2021). NUDT2 initiates viral RNA degradation by removal of 5′-phosphates. Nat. Commun. *12*, 6918. https://doi.org/10.1038/s41467-021-27239-y.

173. Stukalov, A., Girault, V., Grass, V., Karayel, O., Bergant, V., Urban, C., Haas, D.A., Huang, Y., Oubraham, L., Wang, A., et al. (2021). Multilevel proteomics reveals host perturbations by SARS-CoV-2 and SARS-CoV. Nature *594*, 246–252. https://doi.org/10.1038/s41586-021-03493-4.

174. Gebhardt, A., Habjan, M., Benda, C., Meiler, A., Haas, D.A., Hein, M.Y., Mann, A., Mann, M., Habermann, B., and Pichlmair, A. (2015). mRNA export through an additional cap-binding complex consisting of NCBP1 and NCBP3. Nat. Commun. *6*, 8192. https://doi.org/10.1038/ncomms9192.

175. Carvalho, C.M., Polson, N.G., and Scott, J.G. (16–18 Apr 2009). Handling Sparsity via the Horseshoe. In Proceedings of the Twelth International Conference on Artificial Intelligence and Statistics Proceedings of Machine Learning Research, D. van Dyk and M. Welling, eds. (PMLR), pp. 73–80.

176. Stan (2017). Stan stan-dev. Github.io. https://mc-stan.org/.

177. Xu, Y. (2015). Alternating proximal gradient method for sparse nonnegative Tucker decomposition. Math. Prog. Comp. *7*, 39–70. https://doi.org/10.1007/s12532-014-0074-y.

178. Wu, Y.-J. TensorDecompositions.jl: A Julia implementation of tensor decomposition algorithms. GitHub. 2018. https://github.com/yunjhongwu/TensorDecompositions.jl.

179. (2021). R interface to CmdStan. https://mc-stan.org/cmdstanr/.

180. Bhadra, A., Datta, J., Polson, N.G., and Willard, B. (2017). The Horseshoe+ Estimator of Ultra-Sparse Signals. Bayesian Anal. *12*, 1105–1131. https://doi.org/10.1214/16-BA1028.

181. Goeminne, L.J.E., Gevaert, K., and Clement, L. (2016). Peptide-level Robust Ridge Regression Improves Estimation, Sensitivity, and Specificity in Data-dependent Quantitative Label-free Shotgun Proteomics. Mol. Cell. Proteomics *15*, 657–668. https://doi.org/10.1074/mcp.M115.055897.

STAR★METHODS

KEY RESOURCES TABLE

REAGENT or RESOURCE	SOURCE	IDENTIFIER
Antibodies		
NG2/CSPG4 (E3B3G) XP® Rabbit mAb	Cell Signaling	Cat#43916; RRID:AB_3086773
STAT1 Rabbit pAb	Cell Signaling	Cat#9172; RRID:AB_2198300
IFITM3 Rabbit pAb	Proteintech	Cat#11714-1-AP; RRID:AB_2295684
Anti-Influenza A Goat pAb	Millipore	Cat#AB1074; RRID:AB_90475
GAPDH(3E12) Mouse mAb	Bioss USA	Cat#bsm-0978M; RRID:AB_10860217
GPKOW Rabbit pAb	Invitrogen	Cat#PA5-31000; RRID:AB_2548474
beta Actin Antibody (C4) Mouse mAb HRP	Santa Cruz	Cat#sc-47778 HRP; RRID:AB_2714189
Donkey anti-Goat IgG (H+L) Secondary Antibody, HRP	Invitrogen	Cat#PA1-28664; RRID:AB_10990162
Horse Anti-mouse IgG, HRP-linked Antibody	Cell Signaling	Cat#7076; RRID:AB_330924
Goat Anti-Rabbit Immunoglobulins/HRP	Dako	Cat#P0448; RRID:AB_2617138
Bacterial and virus strains		
IAV (Strain: SC35M)	Martin Schwemmle[164] (University of Freiburg, Germany)	N/A
IAVΔNS1 (Strain: SC35M)	Martin Schwemmle[164] (University of Freiburg, Germany)	N/A
IAV Renilla (SC35M NS1_2A_Renilla_2A_NEP)	Peter Reuther[165] (University of Basel, Switzerland)	N/A
SFV-mCherry	Andres Merits (University Tartu, Estonia)	N/A
VACV-V300-GFP	Joachim Bugert (Bundeswehr Institute of Microbiology, Germany)	N/A
Chemicals, peptides, and recombinant proteins		
DMEM (high glucose)	Sigma-Aldrich	Cat#D6429
FBS	Sigma-Aldrich	Cat#F7524
Penicillin-Streptomycin	Sigma-Aldrich	Cat#P4333
DMEM for SILAC	Thermo Scientific	Cat#88364
Fetal Bovine Serum, dialyzed, US origin	Gibco	Cat#26400044
Arg0 (unlabeled L-Arginine hydrochloride powder)	Silantes	Cat#201004102
Lys0 (unlabeled L-Lysine hydrochloride powder)	Silantes	Cat#211004102
Arg10 (13C 15N L-Arginine hydrochloride powder)	Silantes	Cat#201604102
Lys8 (13C 15N L-Lysine hydrochloride powder)	Silantes	Cat#211604102
Arg6 (13C L-Arginine hydrochloride powder)	Silantes	Cat#201204102
Lys4 (2H 4, 4, 5, 5-D4-L-Lysine dihydrochloride powder)	Silantes	Cat#211104113
DMEM (high glucose, no glutamine, no methionine, no cystine)	Gibco	Cat#21013024
L-AHA	Jena	Cat#CLK-AA005
Recombinant human IFN-α	Peter Stäheli (University of Freiburg, Germany)	N/A
Metafectene Pro	Biontex	Cat#T040
Resazurin	Sigma-Aldrich	Cat#R7017
Opti-MEM I Reduced-Serum Medium	Gibco	Cat#31985062
Biotin-PEG4-alkyne	Sigma-Aldrich	Cat#764213
Strep-Tactin® Sepharose® resin	IBA	Cat#2-1201-002
Lysyl Endopeptidase, Mass Spectrometry Grade (Lys-C)	FUJIFILM Wako Chemicals	Cat#12505061

(*Continued on next page*)

CellPress
OPEN ACCESS

Continued

REAGENT or RESOURCE	SOURCE	IDENTIFIER
Sequencing Grade Modified Trypsin	Promega	Cat#V5113
C18 Empore filter discs	Supelco	Cat#66883-U
ReproSil-Pur 120 C18-AQ, 1.9 μm	Dr. Maisch GmbH	Cat#r119.aq.
Critical commercial assays		
Dual-Luciferase Reporter assay	Promega	Cat#E1960
Click-iT™ Protein Reaction Buffer Kit	Invitrogen	Cat#C10276
Deposited data		
human proteome	Uniprot	Taxon ID 9606
IAV H7N7 proteins	Uniprot	Taxon ID 384493
Gene Ontology and Reactome databases	http://download.baderlab.org/EM_Genesets/August_08_2023/Human/UniProt/	N/A
Protein turnover dynamics of IAV-infected HeLa cells	PRIDE	PRIDE: PXD047063
Proteome of GPKOW depleted cells with IAV infection, IFN or PPP-RNA treatment	PRIDE	PRIDE: PXD047060
Experimental models: Cell lines		
HeLa S3	ATCC	CCL-2.2
A549	Georg Kochs (University of Freiburg, Germany)	N/A
293T-Mx1-PLuc	Haas et al.[166]	N/A
Oligonucleotides		
PPP-RNA (IVT4)	Produced in house according to Goldeck et al.[167]	N/A
siRNAs	Qiagen or Dharmacon, see Table S4	N/A
gRNAs	This study, see Table S5	N/A
Recombinant DNA		
WSN mini-replicon system[168]	Georg Kochs[168] (University of Freiburg, Germany)	N/A
EF1α-Ren reporter plasmid	Engin Gürlevik (Hannover Medical School, Germany)	N/A
Software and algorithms		
IncuCyte S3 Software, version 2020C rev1	Essen Bioscience	N/A
ImageLab (v 6.0)	Bio-Rad	N/A
MaxQuant version 1.6.0.15/2.4.8.0	Tyanova et al.[169]	N/A
Cytoscape (v3.9.1)	Shannon et al.[170]	N/A
pcSILAC model and analysis	This study	https://doi.org/10.5281/zenodo.10231157
msglm	This study	https://doi.org/10.5281/zenodo.7752068
msimportr	This study	https://doi.org/10.5281/zenodo.7746897
OptEnrichSetCover	This study	https://doi.org/10.5281/zenodo.4536596
package dependencies for the analysis of this manuscript	This study	https://doi.org/10.5281/zenodo.7752673
Other		
IncuCyte S3 Live-Cell Analysis System	Essen Bioscience	N/A
Q Exactive HF mass spectrometer	Thermo Fisher Scientific	N/A
EASY-nLC 1200 system	Thermo Fisher Scientific	N/A
The protein turnover atlas (interactive homepage containing data from this study)	This study	pulsechase.innatelab.org

EXPERIMENTAL MODEL AND SUBJECT DETAILS

HeLa S3,[171] A549[140] and 293T-Mx1-PLuc (HEK293T stably expressing the firefly luciferase gene under the control of the mouse Mx1 promoter)[166] cells have been described previously. If not specified, the cells were cultured in normal culture medium, which is DMEM (high glucose) supplemented with 10% (v/v) FBS and antibiotics (100 U/ml penicillin, 100 μg/ml streptomycin). The SILAC -L, -H and -M medium was prepared by supplementing DMEM for SILAC with 10% dialyzed FBS, antibiotics (100 U/ml penicillin, 100 μg/ml streptomycin) and 0.8 mM and 0.4 mM of Lys and Arg with the respective weight (L: Lys0, Arg0; H: Lys8 (L-lysine-$^{13}C_6{}^{15}N_2$), Arg10 (L-arginine-$^{13}C_6{}^{15}N_4$); M: Lys4 (L-lysine-D_4), Arg6 (L-arginine-$^{13}C_6$)). The depletion medium for AHA-labeling was prepared by supplementing DMEM (high glucose, no glutamine, no methionine, no cystine, Gibco) with glutamine and cystine, and dialyzed FBS and antibiotics to the same concentration as normal DMEM (high glucose). The AHA-labeling medium was prepared by supplementing the depletion medium further with L-AHA at 0.1 mM.

METHOD DETAILS

IAV WSN mini replicon system

For 0.1 million/well target cells in 24-well plates, 100 ng of each of the three plasmids encoding the subunits of the viral RNA polymerase (PB1, PB2, PA), 200 ng of the plasmid encoding NP and 50 ng of pPOLI-Luc-RT were transfected. The EF1α-Ren plasmid was co-transfected with the mini replicon plasmids and functioned as a transfection control. The virus replication was therefore represented by Firefly/Renilla luciferase activity measured by the Dual-Luciferase Reporter assay.

siRNA knockdown screen

0.1 million/well target cells were seeded in 24-well plates 24 h before the transfection. siRNAs were purchased from Qiagen or Dharmacon (see Table S4) and transfected into the target cells via Metafectene Pro' according to the manufacturer's instructions (15 pmol/well). The transfected cells were either cotransfected with the mini replicon system at the same time or rested for 48 hours before infection by IAV Renilla (MOI 0.02). 36 h post-cotransfection or 24 h post-infection, the respective luminescent signals from the knockdown cells were compared to the respective scrambled control on the same plate. The knockdown of each target gene was repeated in four independent wells for the Renilla infection and three times for the IAV WSN mini replicon. A hit ("strong effect") was defined by Benjamini-Hochberg (BH)-adjusted p-value $\leq$ 0.05 for the IAV Renilla infection in Welch's t-test, or $|\log_2$ fold change$| \geq$ 0.5 in at least two biological replicates for the IAV WSN mini replicon. The GPKOW knockdown and the respective scrambled control after the IAV Renilla infection were further used in the proteomics analysis.

To evaluate the effect of knockdown on cell viability, 1.25×10^4/well of the respective target cells were seeded in 96-well plates for 24 h and transfected with 3.75 pmol/well siRNA in four independent wells as described above. After 48 h, 10 μg of the Resazurin in 100 μl PBS was added to each well directly. The mixture was incubated at 37°C for 30 min and the fluorescence at 535 nm excitation/590 nm emission was recorded as a measure of cell viability. The viability was calculated by dividing the fluorescent signal from knockdown samples by the mean of scrambled control on the same plate. The viability was defined to be affected when the knockdown cells have on average less than 80% of the viability of the scrambled controls, and the BH-adjusted p-value $\leq$ 0.05 for the knockdown vs control comparison.

CRISPR/Cas9 knockdown of GPKOW

The design of guide sequences (see Table S5) against GPKOW and NTCs and their subsequent cloning and lentivirus production was performed as previously described.[172] The lentivirus was used to infect A549 cells for 24 hours and the medium was exchanged with DMEM containing puromycin (1 μg/mL) for 6 days before the subsequent experiments.

Samples for proteomic analysis

For generating samples for mass spectrometry analysis, the cells were seeded at 0.1 million/well in 24-well plates 24 hours before being stimulated with PPP-RNA (200 ng/ml) or IFN-α (100 U/ml) for 10 h. Each condition was repeated in 4 independent wells. The knockdown efficiency was confirmed by the significant downregulation of GPKOW protein abundance compared to the NTC controls.

IFN bioassay

The cells were seeded in 24-well plates 24 hours before being stimulated with PPP-RNA (200 ng/ml). The concentration of IFN-α/β in the supernatants were measured using 293T-Mx1-PLuc cells as described before.[166] The experiment was repeated twice, where each condition was repeated in 4 independent wells.

Infection dynamics with live-imaging analysis

For the infection experiments analyzed by live-imaging, the cells were seeded at 15,000/well in 96-well plates 24 hours before the infection with SFV-mCherry (MOI 3) and VACV-GFP (MOI 0.05) for up to 72 h. The infection experiments were repeated 3 times, each with at 3 independent wells per condition (the combination of virus and gRNA). The live-cell fluorescence imaging was performed by the IncuCyte S3 Live-Cell Analysis System and the images analysis was performed using IncuCyte S3 Software, where

the integrated mCherry or GFP intensity was normalized to the confluence of the cells. The knockdown efficiency of guides used in the virus infection experiments was confirmed by western blot as described before,[173] where the relative intensity of target bands were determined by ImageLab. GPKOW (1:1000), ACTB-HRP (1:2000) and anti-rabbit-IgG (1:2500) antibodies were used.

AHA-methionine pulse experiment

HeLa cells were seeded at 0.8 million per well of 6-well plates in 2 ml of normal culture medium overnight. The next day, the cells were washed twice in PBS, starved in depletion medium for 30 min, then cultured in AHA-labeling medium for 4 hours. Afterwards, the cells were mock-infected or infected by IAV diluted in OptiMEM to a total volume of 200 μl/well for 30 min on ice at MOI of 3 in triplicates, and 2 ml of normal culture medium ("methionine pulse") was added after the infection. The cells were then harvested in 200 μl of lysis buffer (1% SDS in 50 mM Tris-HCl, pH 8.0) at 12, 24 and 36 h.p.i., heated to 95°C for 10 minutes and sonicated for 5 minutes at the high setting. An equal amount of proteins from each sample were subjected to click reaction, where AHA-labeled proteins were clicked to Biotin-PEG4-alkyne via the Click-iT™ Protein Reaction Buffer Kit and extracted according to manufacturer's instructions.

The proteins were dissolved in 200 μl of lysis buffer and the SDS was quenched by 200 μl of NETFD buffer (6% NP-40, 5 mM EDTA, 100 mM NaCl, 50 mM Tris-HCl pH 7.4). 50 μl of Strep-Tactin® Sepharose® resin was added to each sample and the mix was incubated on the rotating wheel at 4°C for 30 min. The beads were washed 3 times with NDTFD buffer and 3 times with NDTF buffer (NETFD without NP-40) and aspirated to dryness. The proteins were released in 50 μl of 2xSSB (4% SDS, 20% Glycerol, 100 mM DTT, 0.02 % Bromophenol blue, 125 mM Tris-HCl, pH 6.8) via heating to 95°C for 10 minutes and analyzed by western blot as described before.[173] CSPG4 (1:1000), STAT1 (1:1000), IFITM3 (1:20000), IAV (1:1000), GAPDH (1:2500), GPKOW (1:1000), ACTB-HRP (1:2000), anti-goat-IgG (1:5000), anti-mouse-IgG (1:2500) and anti-rabbit-IgG (1:2500) antibodies were used.

Integration of the published IAV datasets

The proteins with significantly altered $\tilde{s}$, d_0 or d_1 rates during IAV infection were intersected with IAV interactors defined by five different IAV AP-MS studies without additional filtering[94,97–100] (Figures 3 and S3; Table S3). Similarly, the intersection between protein turnover changes during IAV infection and published genome-wide screens was performed with the selected hit definition of the respective studies without additional filtering[116,126–134] (Figure S4A; Table S3).

QUANTIFICATION AND STATISTICAL ANALYSIS

Sample preparation and data processing

Sample preparation for pcSILAC

HeLa cells were cultured in the SILAC-L medium for two passages before the experiment. The cells were then seeded at 0.8 million per well in 2 ml SILAC-L medium in 6-well plates, rested overnight. The next day, the cells were infected with IAV or IAVΔNS1 viruses diluted in OptiMEM to a total volume of 200 μl/well for 30 min on ice at MOI of 3 in quadruplicates. After the infection, the medium was replaced with the SILAC-H medium (pulse). 12 hours later the medium was further exchanged with the SILAC-M medium (chase). The samples were collected at 12, 18, 24, 30, 36 and 42 hours post-infection for protein lysis subjected to LC-MS/MS analysis. The protein lysis by SDS lysis buffer and subsequent reduction, alkylation, digestion, and purification were performed as described before.[166] To increase the depth of protein detection, a separate group of infections was performed using the same cell type and viruses in quadruplicates. 18 hours after infection, the medium was replaced with the SILAC-M medium, and after another 3 hours (21 h.p.i.), the medium was replaced again with the SILAC-H medium. All the samples were collected at 24 h.p.i., processed the same way as the main samples, and fractionated into 6 fractions to be solely used for matching precursor identifications between MS runs. The data from this group were not included in the downstream analysis.

Sample preparation for full proteome of GPKOW knockdown cells

The GPKOW knockdown HeLa cells with IAV Renilla infection and the GPKOW knockdown A549 cells with IFN-α or PPP-RNA treatment were performed in quadruplicates as described above. The infected knockdown samples were collected after the luminescence measurement and processed in the same way as the pcSILAC samples. The IFN-α or PPP-RNA treated knockdown samples were collected 10 h post-treatment and resuspended in guanidinium chloride buffer (6M guanidiuium chloride in 100mM Tris HCl pH 8.5, 10mM TCEP, 40mM CAA) and heated to 99°C for 15 min. The samples were then diluted 1:10 with 25 mM Tris pH 7.5, 2% ACN and digested with 0.5 μg/ml LysC and 1.25 μg/ml sequencing grade trypsin for 24 h at 30°C. The digested peptides were desalted and concentrated via C18 Empore filter disks as previously described.[174]

LC-MS/MS analysis

All samples were measured on a Q Exactive HF mass spectrometercoupled online to an EASY-nLC 1200 system. The liquid chromatography setup consisted of a 75 μm x 50 cm analytical column, filled with Reprosil Pur C18-AQ 1.9 μm particles. Peptides were separated using a 120/180 min (pcSILAC samples/siRNA-mediated knockdown samples) gradient at a flow rate of 250 nL/min, and a binary buffer system consisting of buffer A 0.1 % (v/v) FA in water, and buffer B 80 % (v/v) ACN, 0.1 % (v/v) FA in water: 2–30% (95/155 min), 30–95% (10 min), wash out at 95% for 5 min, readjustment to 2% in 5 min, and kept at 2% for 5 min. For the CRISPR/Cas9-mediated knockdown samples, peptides were separated using a 180 min gradient at a flow rate of 300 nL/min, and a binary buffer system with the same buffer A and B as described above: 5–30% (150 min), 30–95% (10 min), wash out at 95% for 5 min, readjustment to 5% in 5 min, and kept at 5% for 10 min. The mass spectrometer was operated with the Data-Dependent Acquisition (DDA) technique and in positive ionization mode. Full scan MS1 spectra were obtained across the m/z range of 300 to 1,650 with a

high resolution of 120,000 using an Automatic Gain Control (AGC) target value of 3E6 and a maximum Ion Trap (IT) of 20 milliseconds. For peptide identification, the top 15 peptide precursors were chosen for High-Energy Collision Dissociation (HCD) fragmentation with a normalized collision energy of 27%. The precursor isolation window was set at 1.4 m/z, and MS2 resolution was maintained at 15,000, with an AGC target value of 1E5 and a maximum IT of 25 milliseconds. Only precursors with charge states ranging from 2 to 6 were selected, and dynamic exclusion was enabled with a 20-second window to prevent reselection of recently analyzed precursors.

Processing of raw MS data

The raw files were processed by MaxQuant version 1.6.0.15 (pcSILAC dataset) or 2.4.8.0 (knockdown datasets) using the default setting unless otherwise stated. Label-free quantification (LFQ) and match between run options were enabled in all searches (LFQ min ratio count 2, normalization type classic, protein FDR = 0.01, PSM FDR = 0.01, site FDR = 0.01, max. Missed trypsin site = 2). Spectra were searched against forward and reverse sequences of the human proteome (Uniprot, Taxon ID 9606, release 10.2017 for pcSILAC dataset and release 04.2023 for knockdown datasets) and IAV H7N7 proteins (Uniprot, Taxon ID 384493, release 01.2014 for pcSILAC dataset and release 04.2023 for knockdown datasets) by the built-in Andromeda search engine.[169] For SILAC samples, multiplicity was set to 3, Arg10 and Lys8 were set as heavy label, and Arg6 and Lys4 as medium label parameters. Search results were filtered with a false discovery rate (FDR) of 0.01 for peptide and protein identifications. Intensity values of proteins with SILAC-M labels before the SILAC-M chase, i.e., at 12 h.p.i., were not used for protein turnover modeling.

Statistical analysis of MS data

pcSILAC dynamic system

Our approach to modeling pcSILAC data is based on Jovanovic et al.[6] with several important extensions. The following ordinary differential equations (ODE) model was used to define the dynamics of synthesis and degradation of each protein during the pulse-chase SILAC experiment:

$$\dot{l} = -(d_0+g)l, \quad \dot{\tilde{l}} = -(d_1+g)\tilde{l}+\gamma_L s, \dot{h} = -(d_1+g)h+(\gamma_H I_M+(1-I_M))s, \dot{m} = -(d_1+g)m+I_M s, l(t_0) = l_0, (t_0) = h(t_0) = m(t_0) = 0. \quad (1)$$

Here, $l(t) = \frac{L(t)}{G(t)}$ is the fraction of SILAC-L-labeled molecules of a given protein at timepoint t ($L(t)$) relative to the total amount of the cells at a given time point ($G(t)$). $h(t)$ and $m(t)$ are the fractions of SILAC-H- and M-labeled protein molecules, respectively. $s(t)$ is the synthesis rate (the amount of molecules of a given protein produced at a given moment normalized by the total amount of cells $G(t)$). Two switches of the growth media (the "pulse" at $t_0 = 0$ and the "chase" at t_M) allowed us to separately assess the degradation of proteins that were synthesized before and after the treatment using $d_0(t)$ and $d_1(t)$ degradation rates (the fraction of molecules of a given protein degraded at moment t), respectively. The relative protein abundances l, h, and m, which were normalized by $G(t)$, model the protein intensities measured by LC-MS, since in our experimental workflow we injected the same amount of material for each treatment, timepoint and replicate.

In comparison to Jovanovic et al.,[6] which modeled turnover in postmitotic mouse bone marrow-derived dendritic cells, the ODE (1) includes $g(t) = \frac{\dot{G}(t)}{G(t)}$ to account for cells growth. This updated equation reflects the fact that the reduction in L, H and M levels of a specific protein is a combination of protein degradation and the reduction of a given SILAC label fraction due to the overall cell growth. Indeed, the rate of SILAC-L protein fraction change is

$$\frac{dl}{dt} = \frac{d\left(L/G\right)}{dt} = \frac{(dL)G-(dG)L}{(dt)G^2} = \frac{dL}{dt}\frac{1}{G} - \frac{dG}{dt}\frac{1}{G}\frac{L}{G} = -d_0 L\frac{1}{G} - g\frac{L}{G} = -(d_0+g)l.$$

Additionally, our model accounts for the L-labeled proteins synthesized after "pulsing" using the residual or "recycled" L-labeled amino acids ($\tilde{l}(t)$), so the total proportion of L-labeled proteins is $l(t)+\tilde{l}(t)$. γ_L constant defines the proportion of synthesized "recycled" L-labeled proteins. Similarly, γ_H is the proportion of recycled SILAC-H-labeled proteins synthesized after "chase" event, and the smoothened step function $I_H(t) = \frac{\exp 50(t-t_M)}{1+\exp 50(t-t_M)}$ models the switch from SILAC-H- to SILAC-M-labeled amino acids in the medium at the "chase" timepoint t_M, so that $I_H(t) \approx 0, t < t_M$ and $I_H(t) \approx 1, t > t_M$.

Cell growth rate g(t) *estimation*

We selected a set of reference proteins $\mathcal{P}$, so that for each protein from $\mathcal{P}$, its overall intensity (the sum of all SILAC labels) remains stable over time and their turnover not specifically affected by the treatment (*i.e.* $d_0 = d_1 = d$). To estimate the total amount of cells at a given moment ($G(t)$) we assumed that it is proportional to the total abundance of all reference proteins:

$$G(t) \approx \sum_{p \in \mathcal{P}} (L_p(t) + H_p(t) + M_p(t)).$$

After calculating the derivative and dividing both sides by *G(t)*, we can express the cells growth rate via synthesis and degradation of the reference proteins:

$$g(t) \approx \sum_{p \in \mathcal{P}} \left(- d_p(l_p + h_p + m_p) + s_p \right). (2)$$

By substituting *g(t)* with (2) in the dynamic system (1) and solving (1) simultaneously for all reference proteins, we find their synthesis and degradation rates, and, via (2), *g(t)*.

Fitting pcSILAC dynamic model to the data

The unknown parameters in (1) are the functions $s(t)$, $d_0(t)$, and $d_1(t)$ that define how synthesis and degradation rates of a given protein change over time. While Jovanovic et al.[6] considered only linear functions for these rates, we extended it to a family of sigmoid functions ($r(t)$) defined by the four parameters (p_1, p_2, p_3, and p_4) to allow broader regulation modes:

$$r(t) = r(t|p_1, p_2, p_3, p_4) = \frac{p_3}{1+e^{-(p_1+p_2 t)}} + p_4.$$

To improve the biological interpretation and integration into Bayesian multi-treatment model, $r(t)$ was reparametrized using the values at the beginning and the end of the interval: $r(t) = r(t|\tau_0, \tau_1, r_0, r_1), r_0 = r(0), r_1 = r(T)$ and $\tau_0 = \tau(0) < 0, \tau_1 = \tau(T) > 0$, where $\tau = p_1 + p_2 t$, so

$$p_1 = \tau_0, p_2 = \frac{\tau_1 - \tau_0}{T},$$

$$p_3 = \frac{r_1 - r_0}{(1+e^{-\tau_1})^{-1} - (1+e^{-\tau_0})^{-1}}, p_4 = r_0 - \frac{p_3}{1+e^{-\tau_0}}.$$

Then e.g. the synthesis rate for the *i*-th treatment (*i=1* denotes mock, *i=2* – $IAV_{\Delta NS1}$, and *i=3* – IAV_{WT}) is $s^i(t) = r(t|\tau^i_{s,0}, \tau^i_{s,1}, s^i_0, s^i_1)$. To find the parameters for the synthesis and degradation rates at each condition, we were fitting the ODE model (1) to the measured protein group LFQ intensities of the pcSILAC experiment using the Bayesian approach similar to the one described in Stukalov et al.[173] Briefly, given the initial protein abundance l_0 and the parameters that define $s^i(t)$, $d^i_0(t)$, and $d^i_1(t)$ rates for *i*-th treatment, solving the ODE (1) provides protein intensities for each timepoint and SILAC label. The discrepancy between the predicted and experimentally measured intensities defines the likelihood for a given set of pcSILAC model parameters (the measured intensity for SILAC-L label was matched to $l(t) + \tilde{l}(t)$, the sum of predicted pre-treatment and "recycled" fractions of SILAC-L-labeled proteins). The likelihood was calculated using the same MS signal and missingness model as in Stukalov et al.[173]

Since the initial state of the experimental system is the same for all treatments, we required that the initial turnover rates ($s(0) = s_0$, $d_0(0) = d_1(0) = d_{0,0}$) are the same for all treatments. Considering that the null hypothesis is that treatments do not affect turnover of a particular protein, and that the turnover dynamics is stationary, we used the sparsity inducing horseshoe priors[175] for the rate differences between treatments among the other model parameter priors:

$$d_{0,0} \propto \text{Normal}(0, \sigma_d),$$

$$d^i_{0,1} \propto \text{Normal}(0, \sigma_d), d^1_{0,1} \propto \text{Normal}\left(d_{0,0}, \theta_{d_{0,1}} \lambda^i_{d_{0,1}}\right), i = 1,2,3,$$

$$d^i_{0,1} \propto \text{Normal}\left(d^1_{0,1}, \theta_{d_0} \lambda^i_{d_0}\right), i = 2,3,$$

$$d^i_{1,1} \propto \text{Normal}(0, \sigma_d), d^i_{1,1} \propto \text{Normal}\left(d^i_{0,1}, \theta_{d_1} \lambda^i_{d_1}\right), i = 1,2,3,$$

$$s_0, s^i_1 \propto \text{Normal}(0, \sigma_s), i = 1,2,3,$$

$$s^1_1 \propto \text{Normal}\left(s^1_0, \theta_{s_1} \lambda^i_{s_1}\right),$$

$$s^i_1 \propto \text{Normal}\left(s^1_1, \theta_s \lambda^i_s\right), i = 2,3,$$

$$\tau^i_{d_0,j}, \tau^i_{d_1,j} \propto \text{Normal}\left(0, \sigma_{\tau_d}\right), \tau^i_{s,j} \propto \text{Normal}(0, \sigma_{\tau_s}), i = 1,2,3, j = 0,1,$$

$$\tau^i_{d_0,j} \propto \text{Normal}\left(\tau^1_{d_0,j}, \theta_{\tau_{d_0}} \lambda^i_{\tau_{d_0}}\right), i = 2,3, j = 0,1,$$

$$\tau^i_{d_1,j} \propto \text{Normal}\left(\tau^i_{d_0,j}, \theta_{\tau_{d_1}} \lambda^i_{\tau_{d_1}}\right), i = 1,2,3, j = 0,1,$$

$$\tau^i_{s,j} \propto \text{Normal}\left(\tau^1_{s,j}, \theta_{\tau_s} \lambda^i_{\tau_s}\right), i = 2,3, j = 0,1.$$

The hyperparameters of the model were sampled from the following distributions:

$$\sigma_d \propto \text{Cauchy}^+\left(0, 10^{-2}\right),$$
$$\sigma_s \propto \text{Cauchy}^+\left(0, 10^{-1}\right),$$
$$\theta_{d_0}, \theta_{d_{0,1}}, \theta_{d_1}, \theta_s, \theta_{s_1} \propto \text{Cauchy}^+(0, 1),$$
$$\lambda^i_{d_0}, \lambda^i_{d_{0,1}}, \lambda^i_{d_1}, \lambda^i_s, \lambda^i_{s_1} \propto \text{Cauchy}^+(0, 1), i = 1, 2, 3,$$
$$\sigma_{\tau_d}, \sigma_{\tau_s} \propto \text{Cauchy}^+(0, 1),$$
$$\theta_{\tau_{d_0}}, \theta_{\tau_{d_1}}, \theta_{\tau_s} \propto \text{Cauchy}^+(0, 1),$$
$$\lambda^i_{\tau_{d_0}}, \lambda^i_{\tau_{d_1}}, \lambda^i_{\tau_s} \propto \text{Cauchy}^+(0, 1), i = 1, 2, 3.$$

This Bayesian statistical model was encoded in Stan (version 2.17),[176] the source code is available at https://doi.org/10.5281/zenodo.10231157. The model was separately inferred for each protein group using 4000 warm-up and 4000 sampling MCMC iterations of the 8 independent chains, each 4th sample was used to estimate the posterior distributions of the model parameters and predicted protein intensities.

To estimate the overall intensity of protein synthesis or degradation rate (*r(t)*) for a particular treatment, the following formula was used:

$$r = \int_0^T r(t)\mathrm{d}t = \frac{(1+e^{\tau_0})(1+e^{-\tau_1})}{1 - e^{\tau_0 - \tau_1}} \left(\left(\frac{r_0}{1+e^{-\tau_1}} - r_1 \frac{e^{\tau_0}}{1+e^{\tau_0}} \right) + \ln\left(\frac{1+e^{\tau_1}}{1+e^{\tau_0}} \right) \frac{r_1 - r_0}{\tau_1 - \tau_0} \right).$$

Synthesis rates for proteins of different abundance classes vary considerably, to make them comparable we divided *s* by the initial abundance of the protein (I_0). Infection-dependent host translation shutoff and cellular stress results in overall reduction of protein synthesis. To detect statistically significant treatment-dependent changes to protein turnover beyond this trend, we further corrected the abundance-scaled synthesis rates by their median for each treatment:

$$\tilde{s}^i_n = \left(\underset{m = 1,2,\ldots,N}{\text{median}} \frac{s^i_m}{I_{m,0}} \right)^{-1} \frac{s^i_n}{I_{n,0}}, n = 1, 2, \ldots, N,$$

where *i* is the treatment, and *n* is the protein group index.

Dimensionality reduction analysis of pcSILAC data

To identify global turnover patterns across all treatments, we first converted the protein group LFQ intensities into 3D tensor, with the first axis being experiment timepoints and SILAC labels, the second – treatments and replicates, and the third – protein groups. Only the proteins that have at least 10 intensity measurements in any SILAC label were considered for this analysis, resulting in 5688 protein groups. Missing values were imputed by sampling from the posterior distribution of model-predicted protein intensities. The intensities were normalized along the third axis by the initial intensity of the protein (I_0 model parameter).

We then applied sparsity-inducing semi-nonnegative Tucker decomposition[177] as implemented in TensorDecompositions.jl Julia Package (version 0.5.0).[178] The core tensor was allowed to contain negative values, its size was set to 16×5×40. The regularization terms for the core tensor and the non-negative factor matrices were all set to 10^{-2}.

The third factor matrix of the Tucker decomposition (the one describing individual protein groups) was then used as an input for the UMAP algorithm (uwot R package) using the default parameters except *neighbors*=100, and *init=''laplacian''.* The 2D UMAP was used for the visualization. By cutting the hierarchical clustering (built using Euclidean distance with Ward linkage) of the 4D UMAP coordinates we distributed protein groups into 50 clusters by their turnover dynamics across all treatments. The source code for the dimension reduction analysis is available at https://doi.org/10.5281/zenodo.10231157.

Full proteome of GPKOW knockdown cells

The MaxQuant output files were imported into the R environment using the custom msimportr R package(https://doi.org/10.5281/zenodo.7746897). This package formats evidence.txt, peptides.txt, and proteinGroups.txt without any filtering for the subsequent analysis with the msglm package(https://doi.org/10.5281/zenodo.7752068), as previously described.[173] The protein groups were redefined using in-house Julia module (https://doi.org/10.5281/zenodo.7752673). In brief, protein groups distinguished by only one specific peptide or if less than 25% of their peptides are specific were merged. This extended the set of peptides used for protein group quantitation and reduced isoform-specific protein groups with insufficient quantitative data. The msglm package applies MS-specific Bayesian linear models to deduce changes in protein abundance across different experimental conditions via the use of cmdstanr package (version 0.4.0).[179] Since most of the cellular proteins are not expected to respond to the different treatments, the model uses regularized sparsity-inducing horseshoe+ priors[180] for the effects associated with experimental conditions.

The probability of quantifying a peptide increases with its intensity, thus we first evaluated the measurement error of our MS instrument by fitting a heteroscedastic intensity noise model, assuming that quanted intensities follow a mixture of Gaussian and Cauchy distributions. This model was calibrated using technical replicate measurements of the MS instrument. We then used the same data

to calibrate a logit-based model of missing MS data, estimating the likelihood of having missing data given the true intensity of an object. Msglm thus handles both quantified and missing values, as both influence the posterior distribution of model parameters, and does not rely on imputation.

Instead of normalizing the input data beforehand, the model was applied to unnormalized MS1 intensities of protein group specific peaks (from the evidence.txt table of the MaxQuant output) to better account for the signal-to-noise variation among samples. The inferred protein abundances were then scaled by the normalization multiplier of each individual MS sample to match its expected MS intensity. To calculate the multiplier, normalization factors were first deduced for individual MS1 peaks by dividing the intensity from different samples to the median of the intensity. Then the median of the normalization factors within each sample was chosen as the normalization multiplier.

For the estimation of model parameters, 4,000 iterations were employed, divided into 2,000 warmup iterations followed by 2,000 sampling iterations. These iterations were executed using the no-U-turn Markov Chain Monte Carlo algorithm in eight independent chains. To assess the significance of differences between conditions, p-values were computed by measuring the probability that two random samples from the respective posterior distributions of two different conditions were distinct. Notably, there was no correction for multiple hypothesis testing, as this was resolved through the selection of model priors.

The model for the proteome analysis of siRNA-mediated GPKOW knockdown infection can be represented by R GLM formula language as

$$\log(Intensity(t)) \sim 1 + knockdown + MS1peak,$$

and of CRISPR/Cas9-mediated GPKOW knockdown with PPP-RNA or IFN-α treatment as

$$\log(Intensity(t)) \sim 1 + treatment * knockout + MS1peak,$$

MS1peak is the log ratio of an MS1 peak intensity and the total protein abundance.[173] The peak represents a peptide with a specific sequence, PTMs and charge, and the log ratio is assumed to be constant regardless of the experimental conditions.[181]

For any comparison between two conditions to be valid, we required the protein group to be quantified in at least three out of four replicates on either side of the comparison. A significant change at any given time was defined by |median ($\log_2$ fold change)| $\geq$ 0.5 and p-value $\leq 10^{-3}$. The source code for the proteome analysis is available at https://doi.org/10.5281/zenodo.10231157.

Pathway enrichment analysis

Proteins from different clusters of the hierarchical clustering analysis (Figure 1F) and proteins with significantly altered $\tilde{s}$, d_0 or d_1 rates in IAV and IAVΔNS1 infections (Figure 2B) were used for the enrichment analysis against the Gene Ontology and Reactome databases (version 2023.08, http://download.baderlab.org/EM_Genesets/August_08_2023/Human/UniProt/) via the in-house Julia package OptEnrichedSetCover.jl (https://doi.org/10.5281/zenodo.4536596) as previously described.[173] No multiple hypotheses correction to the FET p-values was done, since the selection of the most relevant non-redundant enriched terms is a part of the method, and it dramatically shortens the list of reported terms. Terms with unadjusted FET p-value $\leq 10^{-4}$ (Figure1F) or 10^{-3} (Figure 2B) were displayed. In the heatmaps, the enriched terms and the conditions are clustered via hierarchical clustering with Ward linkage method and cosine distance.

For Figures 2C and S2E, proteins with significantly altered degradation (d_0) and their degradation change during IAV infection were supplied to the Gene Set Expression Analysis[93] of the ReactomeFIViz plugin in Cytoscape (v3.9.1),[170] using default settings and Reactome FI Network Version 2021 for clustering. After that, a pathway enrichment analysis from the Reactome plugin was performed for each cluster, and a selection of terms with FDR $\leq$ 0.001 were displayed.